

Title

Calibration of the NDHA model to describe N₂O dynamics from respirometric assays.

Author list

Carlos Domingo-Félez^a, María Calderó-Pascual^a, Gürkan Sin^b, Benedek G. Plósz^{a,l}, Barth F. Smets^{a*}

^aDepartment of Environmental Engineering, Technical University of Denmark, Miljøvej 115, 2800 Kgs. Lyngby, Denmark

^bDepartment of Chemical and Biochemical Engineering, Technical University of Denmark, Søltofts Plads 229, 2800 Kgs. Lyngby, Denmark

^lPresent address: Department of Chemical Engineering, University of Bath, Bath, England.

* Corresponding author:

Barth F. Smets, Phone: +45 4525 1600, Fax: +45 4593 2850, E-mail: b fsm@env.dtu.dk

Abstract

The NDHA model comprehensively describes nitrous oxide (N₂O) producing pathways by both autotrophic ammonium oxidizing and heterotrophic bacteria. The model was calibrated via a set of targeted extant respirometric assays using enriched nitrifying biomass from a lab-scale reactor. Biomass response to ammonium, hydroxylamine, nitrite and N₂O additions under aerobic and anaerobic conditions were tracked with continuous measurement of dissolved oxygen (DO) and N₂O.

The sequential addition of substrate pulses allowed the isolation of oxygen-consuming processes. The parameters to be estimated were determined by the information content of the datasets using identifiability analysis. Dynamic DO profiles were used to calibrate five parameters corresponding to endogenous, nitrite oxidation and ammonium oxidation processes. The subsequent N₂O calibration was not significantly affected by the uncertainty propagated from the DO calibration because of the high accuracy of the estimates. Five parameters describing the individual contribution of three biological N₂O pathways were estimated accurately (variance/mean < 10% for all estimated parameters).

The NDHA model response was evaluated with statistical metrics (F-test, autocorrelation function). The 95% confidence intervals of DO and N₂O predictions based on the uncertainty obtained during calibration are studied for the first time. The measured data fall within the 95% confidence interval of the predictions, indicating a good model description. Overall, accurate parameter estimation and identifiability analysis of ammonium removal significantly decreases the uncertainty propagated to N₂O production, which is expected to benefit N₂O model discrimination studies and reliable full scale applications.

Keywords: Nitrous oxide, Respirometry, Accuracy, Modelling, Parameter Estimation

Highlights

- An experimental design to calibrate N₂O models via extant respirometry is proposed.
- Parameters associated to N₂O production were identified accurately (CV < 10%).
- The NDHA model described N₂O production at varying DO and HNO₂ concentrations.
- The uncertainty of the N₂O emission factor in a case study was ~ 10% of its value.

1. Introduction

Nitrous oxide (N_2O) is a greenhouse gas emitted during biological nitrogen removal (BNR). The carbon footprint of wastewater treatment plants (WWTPs) is highly sensitive to N_2O emissions (Gustavsson and Tumlin, 2013), thus reducing N_2O emissions is beneficial for the energy balance of WWTPs.

During BNR operations biological and abiotic pathways are responsible of N_2O emissions (Schreiber et al., 2012). Ammonia-oxidizing bacteria (AOB) produce N_2O during incomplete ammonium (NH_4^+) oxidation to nitrite (NO_2^-) (nitrifier nitrification, NN). Under low dissolved oxygen (DO) AOBs use NO_2^- as the terminal electron acceptor and also release N_2O (nitrifier denitrification, ND). Heterotrophic denitrification is a 4-step process where N_2O is an obligate intermediate. Under low carbon-to-nitrogen ratios or in the presence of DO heterotrophic denitrification is not complete and N_2O can be released (HD) (Richardson et al., 2009). Hydroxylamine (NH_2OH) and free nitrous acid (HNO_2) are intermediates of NH_4^+ oxidation which can produce N_2O abiotically.

Process models are useful tools that translate our understanding of N_2O production into mathematical equations. N_2O model structures vary depending on the number of pathways, nitrogenous variables or parameters considered (Ding et al., 2016; Ni et al., 2014; Pocquet et al., 2016). The description of the autotrophic contribution transitioned from single- (NN or ND) to two-pathway (NN and ND) models to capture the N_2O dynamics observed during N-removal (Pocquet et al., 2016; Schreiber et al., 2009). Recently, a consistent N_2O model was proposed (NDHA) that predict three biological pathways and abiotic processes (Domingo-Félez and Smets, 2016). Potentially, the NDHA model describes N_2O production under a wide range of operational conditions.

N_2O models are extensions of existing structures describing nitrogen removal and thus, calibration of N_2O dynamics also requires accurate predictions of the primary substrates (i.e. DO, NH_4^+ , NO_2^- , etc.). The experimental datasets used for calibration in lab-scale systems are either directly obtained from the reactor performance (Ding et al., 2016) or by conducting batch experiments (Ni et al., 2011). Initially, the information content of the experimental design was not studied because models aimed at describing N_2O trends without focusing on rigorous calibrations (Law et al., 2011). However, the amount and quality of data of the experimental design directly impact the calibration results (Dochain and Vanrolleghem, 2001).

Some studies report the proposed calibration framework (Guo and Vanrolleghem, 2014), but the N_2O parameter estimation procedures are often ill-described, with little information about each step. For example, the parameter subset selection considered during parameter estimation is

sometimes not addressed. Local sensitivity measures are used as rankings for parameter selection (Pocquet et al., 2016; Spérandio et al., 2016), but these rankings are dependent on the initial parameter values and do not capture parameter interactions (Brun et al., 2001).

The overall fit and capabilities to describe N₂O dynamics has relied on analysis from best-fit simulations (e.g. R²), which can lead to ambiguous results that cannot discriminate between models (Lang et al., 2017; Pan et al., 2015). A more rigorous analysis of residuals (e.g. Gaussian distributions, autocorrelation functions (ACF), F-test, etc.) would benefit the validation of the model response (Bennett et al., 2013).

Also, addressing the practical identifiability of newly estimated parameters will improve N₂O model discriminations procedures. For example, the parameter variance and correlation matrix are indicators of the confidence that can be given to a value, but they are not always reported, which makes it difficult to compare between N₂O model predictions (Ding et al., 2016; Kim et al., 2017; Pocquet et al., 2016; Spérandio et al., 2016). Practical identifiability problems might contribute to the large variability of parameter values in N₂O models (Domingo-Félez et al., 2017).

The uncertainty obtained during calibration translates into confidence intervals for model predictions. The accuracy, or width of the confidence interval, associated to the N₂O emissions will be a key factor to consider during the development of mitigation strategies. Yet, the uncertainty of N₂O emissions associated to model calibration is not studied.

The objective of this study is to demonstrate and evaluate a standardized procedure for parameter estimation from N₂O models that relies on respirometric assays and in particular its application to analyse and validate the recently developed NDHA models. These assays are designed to allow the sequential fit of model components. The novelty resides in improving N₂O calibration procedures by targeting sources of uncertainty. Subsequently, the calibration results and associated uncertainty are evaluated. The calibration approach presented is a rigorous tool beneficial for N₂O model discrimination.

2. Material and Methods

2.1. Experimental Design

Nitrifying enrichment culture.

A lab-scale nitrifying sequencing batch reactor (5 L) was operated and displayed stable performance for three months after enrichment from an AS mixed liquor sample. Synthetic wastewater (modified after Graaf et al., 1996) with NH_4^+ as the only nutrient was fed at 0.5 g NH_4^+ -N/L-d and a constant aeration rate maintained oxygen-limited conditions (DO below 0.25 mg/L) (SI-S1). NH_4^+ removal was $82 \pm 14\%$, and nitrification efficiency ($\text{NO}_2^-/\text{NH}_4^+$ removed) at $85 \pm 24\%$. The biomass composition, based on 16 rRNA targeted qPCR analysis had a dominance of AOB over NOB (30:1). Detailed information of the qPCR analysis can be found in (Terada et al., 2010).

Monitoring nitrification and N_2O production via extant respirometric assays.

Biomass samples were harvested towards the end of the react cycle by centrifugation at 3600 g for 5 min, washed and resuspended in nitrogen-free mineral medium three times to eliminate any soluble substrate.

Assays were performed in parallel at 25°C in two 400-mL jacketed glass vessels completely filled with biomass and sealed with the insertion of a Clark-type polarographic DO electrode (YSI Model 5331, Yellow Springs, OH). Biomass samples were saturated with air or pure oxygen prior to the initiation of the respirometric assays. A decrease in the DO level in the vessel due to substrate oxidation was measured by the DO probe and continuously acquired by a personal computer interfaced to a DO monitor (YSI Model 5300, Yellow Springs, OH) by a multi-channel data acquisition device (LabPC+, National Instruments, Austin, TX). DO profiles were acquired at a user-defined frequency below the response time of the sensor (0.2 Hz). Liquid N_2O concentrations were measured with Clark-type microsensors (N2O-R, Unisense A/S, Aarhus, Denmark) and pH (WTW GmbH, Weilheim, Germany). Stock solutions for all the reagents were prepared from high-purity chemicals for NH_4HCO_3 , $\text{NH}_2\text{OH}\cdot\text{HCl}$, NaNO_2 , $\text{C}_3\text{H}_5\text{NaO}_2$ (Sigma Aldrich) and by sparging $\geq 99.998\%$ gas in deionized water for N_2O (Sigma-Aldrich).

Table 1 – Experimental design for respirometric assays. Grey shading corresponds to anoxic experiments.

Scenario	Substrate added	Targeted processes	N ₂ O pathways
Scen_AMO	NH ₄ ⁺	NH ₄ ⁺ removal by AOB N ₂ O production at excess/limiting DO (NH ₄ ⁺ excess)	NN, ND
Scen_AMO_DO	NH ₄ ⁺	Low DO part of Scen_AMO	
Scen_HAO	NH ₂ OH	NH ₂ OH removal by AOB N ₂ O production at excess/limiting DO (NH ₂ OH excess)	NN, ND
Scen_NOB	NO ₂ ⁻	NO ₂ ⁻ removal by NOB N ₂ O production at excess/limiting DO (NO ₂ ⁻ excess)	HD
Scen_An_AOB	NH ₄ ⁺ , NH ₂ OH, NO ₂ ⁻	Role of NH ₄ ⁺ , NH ₂ OH, NO ₂ ⁻ on AOB-driven N ₂ O production	NN, ND
Scen_An_HB	N ₂ O, NO ₂ ⁻ /NO ₃ ⁻	Role of N ₂ O, NO ₂ ⁻ and NO ₃ ⁻ on HB-driven N ₂ O production	HD

Experimental Design

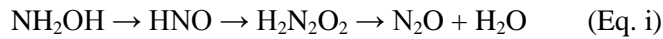
The aim of the experimental design was to obtain informative data on N₂O dynamics for a nitrifier dominated biomass to allow estimation of parameters of the NDHA model, which captures processes associated with nitrification, denitrification, and abiotic processes. Respirometric approaches were exclusively taken (on-line, high-rate O₂ and N₂O measurements) as they allow accurate parameter estimates compared to substrate depletion experiments (Chandran et al., 2008). The kinetics of the oxidation of the primary N-substrates (NH₄⁺, NH₂OH and NO₂⁻) were individually and step-wise, measured via extant respirometry under various initial DO conditions, with continuous N₂O measurements (Table 1). Then the interaction between the different N species was ascertained. In addition, specific experiments were conducted to measure the heterotrophic and abiotic contributions to total N₂O production during nitrification.

The purpose was to predict the fate of the primary N-substrates based on the specific oxygen-consuming rate. By sequentially adding substrate pulses from oxidized to reduced form (NO₂⁻ → NH₂OH → NH₄⁺), the individual rates can be isolated. The N₂O dynamics from NH₄⁺ removal at varying NO₂⁻ and DO concentrations can be investigated simultaneously.

2.2. N₂O model description: NDHA

The NDHA model was proposed as a consilient model to describe N₂O dynamics under a variety of conditions for biomass containing both autotrophic and heterotrophic fractions (Domingo-Félez and Smets, 2016). It considers N₂O production from two autotrophic and one heterotrophic biological pathways, plus abiotic N₂O formation based on recent findings (Soler-Jofra et al., 2016). Unlike any other model, NDHA can qualitatively capture NO and N₂O profiles that have observed at high and low DO (Castro-Barros et al., 2016; Kampschreur et al., 2008; Rodriguez-Caballero and Pijuan, 2013; Yu et al., 2010). Here we aim to calibrate the NDHA model.

The following summarizes the essential and unique components of NDHA; for more information see (Domingo-Félez and Smets, 2016). The two autotrophic pathways have two different NO-producing processes, which are combined into a single N₂O-producing process. In Nitrifier Nitrification (NN), NO_{NN} is produced during NH₄⁺ oxidation (AOR) under oxic conditions. Higher AOR will likely increase NO_{NN} and also N₂O. A fraction of NH₄⁺, proportional to AOR is always released as N₂O_{NN}. In autotrophic denitrification (ND), under low DO NO_{ND} is produced by the reduction of HNO₂ with NH₂OH. This step is negatively affected by DO. The reduction of both NO_{ND} and NO_{NN} is lumped in one process with no oxygen inhibition as it is not known whether both NIR and NOR steps are directly inhibited by DO (Kozłowski et al., 2014). Thus, if NIR is inhibited by DO the overall ND-associated N₂O production will be indirectly limited. The 4-step denitrification model was considered based on (Hiatt and Grady, 2008). Individual process rates and inhibition/substrate coefficients were used as suggested for systems with low substrate accumulation. Nitrification produces HNO₂ and NH₂OH. Abiotically NH₂OH can form HNO which dimerizes via H₂N₂O₂ to N₂O and H₂O (Eq. i). HNO accumulation could occur due to an imbalance between the two reactions, leading to chemical N₂O production (Igarashi et al., 1997). Nitrosation of NH₂OH (Eq. ii) has also been postulated as a relevant reaction in partial nitrification reactors (Soler-Jofra et al., 2016).



2.3. Parameter estimation procedure

The steps in the parameter estimation procedure were to (1) estimate the best fit parameters to describe O₂ consumption and N₂O production during the various (or during each type of) experimental scenarios (Figure 1), (2) estimate the contribution of separate pathways to the total N₂O production, and (3) quantify the uncertainty of model predictions.

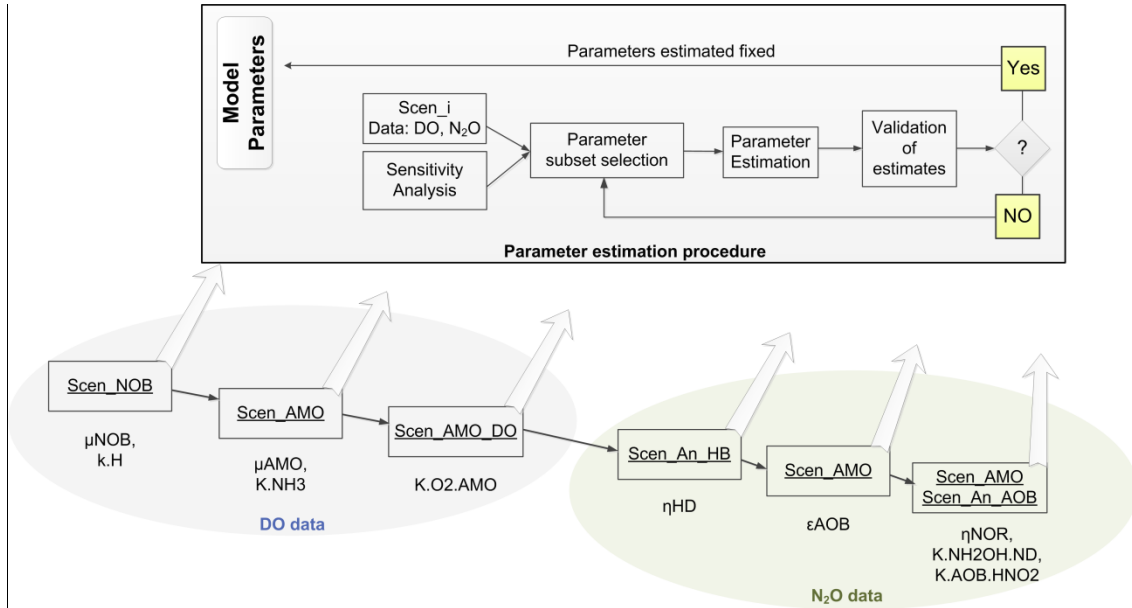


Figure 1 – Schematic of the parameter estimation procedure.

2.3.1. Scenarios (Batches grouped by substrate added: NH_4^+ , NH_2OH , NO_2^-)

A scenario (e.g. Scen_AMO) was defined as a group of experiments with the same primary N-substrate added by pulses (Table 1). The overall oxygen consumption was the additive effect of several independent oxygen consumption processes, potentially including endogenous -, NO_2^- -, NH_2OH -, and NH_4^+ -respiration. By sequentially following the respirometric response from more to less oxidized state N-substrates (i.e., first NO_2^- , then NH_2OH , then NH_4^+), the identifiability of nitrification kinetic parameters increases as steps can be estimated sequentially (Brouwer et al., 1998).

2.3.2. Parameter estimation

The error function for problem minimization was defined as:

$$\text{Error} = \sum_j^m \frac{1}{n} \sum_i^n \left(\frac{y_{sim,i} - y_{obs,i}}{\sigma_i} \right)^2$$

Where m is the number of experiments in one scenario (e.g. 2 NOB experiments in Scen_NOB), n the number of experimental points of each experiment, $y_{sim,i}$ the model prediction and $y_{obs,i}$ the experimental data at time i , and σ_i the standard error of the experimental data. The minimization problem was started with global search method over a wide parameter space (GlobalSearch algorithm). From the estimated minimum, multiple local searches (PatternSearch algorithm) were started randomly in a narrower parameter space to avoid local minima. Model simulations were performed in the Matlab environment (The Mathworks Inc., Natick, USA).

2.3.3. Parameter subset selection - Global sensitivity analysis

A global sensitivity analysis was performed to identify the parameters most determinant of model outputs by linear regression of Monte-Carlo simulations (Sin et al., 2009). Uncertainty from model parameters was propagated as 10-25-50% uniform variations from their default value to model outputs (SI-S2). Latin hypercube sampling was used to cover the parameter space. The Standardized Regression Coefficient method was used to calculate the sensitivity measure β_i , which indicates the effect of the parameter on the corresponding model output (Campolongo and Saltelli, 1997) (convergence found with 500 samples).

Parameters describing the elemental biomass composition (e.g. i_{NXB}), yield and temperature coefficients were fixed at default values and not considered for calibration. For each scenario the top ranked most sensitive parameters were preliminary selected as candidates for parameter estimation. All possible combinations of parameter candidates were assessed by increasing the size of the calibration subset to find the largest identifiable subset with the lowest error, assessed by the Akaike Information Criterion (AIC) (Akaike, 1974). To compare the information content of different parameter subsets of the same size the optimal experimental design criteria *modE* (Dochain and Vanrolleghem, 2001) was calculated together with RDE, which captures the accuracy and precision of a calibrated subset (Machado et al., 2009). Newly estimated parameters were fixed at their best-fit estimate on the next calibration step (Figure 1).

2.3.4. Validation of model response and parameter estimates

To test the validity of the model response (i.e. the adequacy of model to predict the observed data points) the residuals ($y_{sim,i} - y_{obs,i}$) were compared to a Gaussian distribution with a one-sample Kolmogorov-Smirnov test (Lilliefors, 1967). Interdependency of residuals was analysed by autocorrelation for different lag times (Cierkens et al., 2012). The quality of the model fit was calculated via correlation coefficients (R^2) and challenging the hypothesis of the linear regression with simultaneous unit slope and zero intercept, where a value of 0/1 indicates a bad/good model fit (F-test). Moreover, by separating the error into three components: means, slope differences and randomness the Mean Squared Error Prediction (MSEP) index identifies the main error source between randomness, mean and standard deviation of residuals (NC, ME, SE) (Haefner, 2005). The prediction accuracy and the validation of the model to individual experiments was evaluated by the Root Mean Squared Error (RMSE) and the Janus coefficient to compare the RMSE between model calibration and validation (Power, 1993).

Based on the Fisher Information Matrix (FIM) collinearity indices were calculated to evaluate the identifiability of parameter estimates (Brun et al., 2001). Approximate confidence regions were calculated following $J_{crit} = J_{opt} \left(1 + \frac{p}{N_{data}-p} F_{\alpha,p,N_{data}-p} \right)$ (Beale, 1960). Coefficients of

variation (CV) were described as the ration between the variance (σ) and the mean (μ) of the estimate.

The reliability of predictive distributions (95% confidence intervals) was evaluated by calculating the Percentage of observations within the Unit Confidence Interval (PUCI) (Li et al., 2011), which combines the fraction of experimental points inside the confidence interval (PCI) and the Average Relative Interval Length (ARIL) $ARIL_{0.95} = \overline{(\text{Limit}_{\text{Upper},0.95} - \text{Limit}_{\text{Lower},0.95})} / \text{Data}$ (Jin et al., 2010). A smaller ARIL value (narrow distance between upper and lower 95% CI predictions) and a larger PUCI represent a better performance.

2.4. Uncertainty evaluation

The effect of directly estimated versus assumed parameter uncertainty was evaluated by Monte-Carlo simulations. The parameter distribution was sampled via LHS ($n = 500$) for two cases: from the distributions obtained during calibration, and compared to uncertainty classes assumed from literature as a reference case (Sin et al., 2009). The resolution of prediction uncertainty was assessed by the ARIL.

3. Results

3.1. Oxygen consumption during respirometric assays.

Each scenario grouped experiments based on the substrate added: NO_2^- (Scen_NOB) NH_2OH (Scen_HAO) or NH_4^+ (Scen_AMO). In all scenarios, even prior to any substrate spikes, oxygen consumption was always positive and proportional to the biomass concentration due to endogenous respiration. After substrate addition, oxygen consumption increased, to a much higher rate with NH_4^+ or NH_2OH than with NO_2^- spikes (Figure 2). The lower NO_2^- oxidizing rate of the biomass agreed with the measured low NOB vs AOB abundance (ca. 1:30).

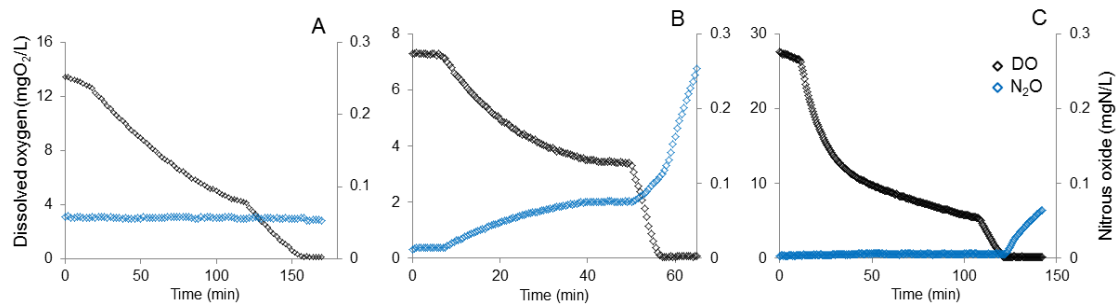


Figure 2 – Dissolved oxygen and liquid nitrous oxide concentrations during experiments: Scen_NOB (NO_2^- pulses) (A), Scen_HAO (NH_2OH pulses) (B) and Scen_AMO (NH_4^+ pulses) (C) (3-4.5 mgN/L).

The ranking from the global sensitivity analysis for DO shows that the sequential scenarios (measuring the respirometric response to addition of synthetic substrates) provides sufficient information to individually estimate the relevant biokinetic parameters of each step in the ammonium oxidation process (Figure 3). For example, in Scen_NOB the maximum growth rate for NOB (μ_{NOB}) ranked first, while in Scen_AMO the substrate affinity ($K_{\text{AOB.NH}_3}$) and maximum growth rate for the AMO ($\mu_{\text{AOB.AMO}}$) step ranked in the top.

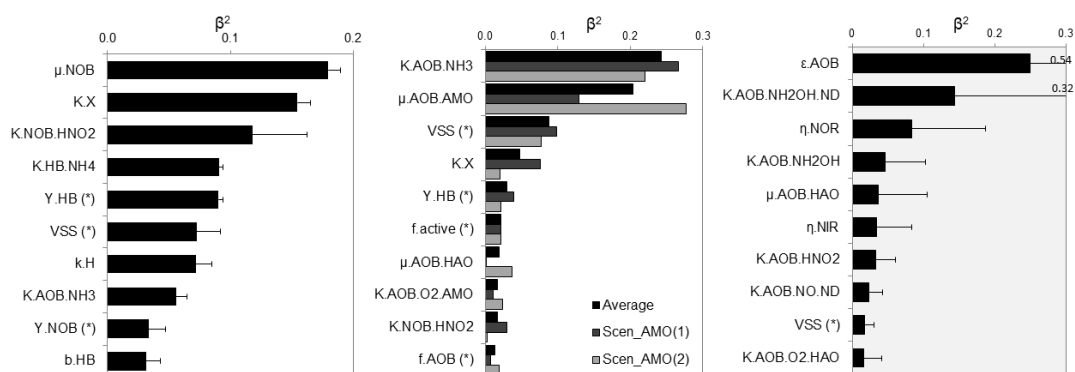


Figure 3 – Parameter sensitivity ranking of scenarios used during calibration for DO (white background) and N_2O (grey background). Scen_NOB (left), Scen_AMO (middle and right). (*) Parameters not considered for calibration.

3.1.1. Estimation of primary substrate kinetics based on DO profiles

Initial conditions for each batch were defined by simulating endogenous decay and hydrolysis with default parameters. The objective of the parameter subset selection was to calibrate the minimum number of identifiable parameters that explain the data. The calibrated parameters for Scen_NOB were μ_{NOB} and k_{H} , for Scen_AMO μ_{AMO} and $K_{\text{AOB.NH}_3}$, and for Scen_AMO_DO $K_{\text{AOB.O}_2.\text{AMO}}$ (Table 2). To illustrate the procedure used for every scenario results from Scen_NOB and Scen_AMO are summarized in the SI (SI-S3). The electron distribution in AOB differs between NH_4^+ (Scen_AMO) oxidation and isolated NH_2OH oxidation (Scen_HAO) (SI-S4). Hence, parameter estimation results from Scen_HAO were not considered representative of NH_4^+ oxidation, our targeted process. To describe more accurately the low NH_2OH concentration values reported in literature (Soler-Jofra et al., 2016) the affinity for NH_2OH , $K_{\text{AOB.NH}_2\text{OH}}$, was increased compared to other N_2O models (SI-S4). The proposed higher affinity for NH_2OH agrees with the lack a slower oxygen consumption rate after NH_4^+ depletion that would indicate NH_2OH accumulation (3.43 vs 2.29 mgCOD/mgN) (Figure 2, right).

Table 2 – Estimated parameters for each scenario (corrected for $T = 20\text{ }^\circ\text{C}$). CV - coefficient of variation = variance / mean; Correlation – correlation coefficient of parameter estimates from the same scenario; RMSE – root mean squared error.

	Scenario	Parameters	Units	Best-fit	CV	Correlation	RMSE	
DO data	NOB	μ_{NOB}	1/d	0.67	1.0%	1	-0.55	0.37
		k_{H}	1/d	2.01	0.9%	-0.55	1	
	AMO	$\mu_{\text{AOB.AMO}}$	1/d	0.49	2.0%	1	0.89	0.39
		$K_{\text{AOB.NH}_3}$	mgN/L	0.12	3.9%	0.89	1	
	AMO_DO	$K_{\text{AOB.O}_2.\text{AMO}}$	mgO ₂ /L	0.23	7.0%		0.08	
N ₂ O data	An_HB	η_{HD}	(-)	0.055	0.7%			0.03
	AMO	ϵ_{AOB}	(-)	0.00048	1.1%			0.001
	AMO / An_AOB	$K_{\text{AOB.HNO}_2}$	$\mu\text{gN/L}$	0.67	4.4%			0.002
		η_{NOR}	(-)	0.16	3.2%	1	0.98	0.002
		$K_{\text{AOB.NH}_2\text{OH.ND}}$	mgN/L	0.25	1.8%	0.98	1	

Validation of model response (DO) and primary N-substrate parameter estimates

The model consistently described the experimental DO profiles for every scenario (F-test = 1, which indicates that we fail to reject the null hypothesis of slope 1 and intercept 0 between simulations and observations) (Figure 4, A, B). The MSEP indicated that randomness was the main source of error compared to the mean or standard deviation, validating the model response during calibration (NC > ME, SE, SI-S5). The uncertainty of the parameter estimates (Table 2) was propagated to the model predictions, showing an increased resolution of the 95% predictive distributions for DO compared to the uncertainty of the reference case (ARIL = 3.8/0.5

before/after parameter estimation). The PUCI (percentage of observations bracketed by the unit confidence interval) also improved from 0.4 to 1.5.

Best-fit parameter estimates at each scenario were estimated at high accuracy: coefficients of variation (CV) were below 7% for all cases (Table 2) and the collinearity indices below 15, as suggested for identifiable subsets (Brun et al., 2002) (SI-S3). The high correlation between $\mu_{\text{AOB.AMO}}-K_{\text{AOB.NH}_3}$ typically occurs for Monod-type kinetics but it did not affect their identifiability.

While the error distribution of each scenario was not normally distributed (Kolmogorov-Smirnov test 95%), no systematic deviations were observed (Figure 4). The analysis of the residuals indicated that for scenarios AMO and NOB the errors were autocorrelated (SI-S5). Subsequently, the effect of sampling resolution on the optimal parameter values and uncertainties was minimized until the autocorrelation obtained was negligible (SI-S5). As the sampling data frequency decreased through subsampling, the accuracy of estimates decreased too (e.g. $\text{CV}_{\mu_{\text{AOB.AMO}}} = 2\%$ point/2 min, 4.4% point/10min). However, the lower precision of the best-fit estimates did not translate into higher simulation uncertainty for the primary N-substrates ($\sigma_{95\% \text{CI}}$ increased by less than 0.06 mg/L for DO, NH_4^+ , NH_2OH or NO_2^-). Consequently, while the autocorrelation of residuals affected the DO parameter estimation results it did not impact the N_2O calibration, the focus of this study.

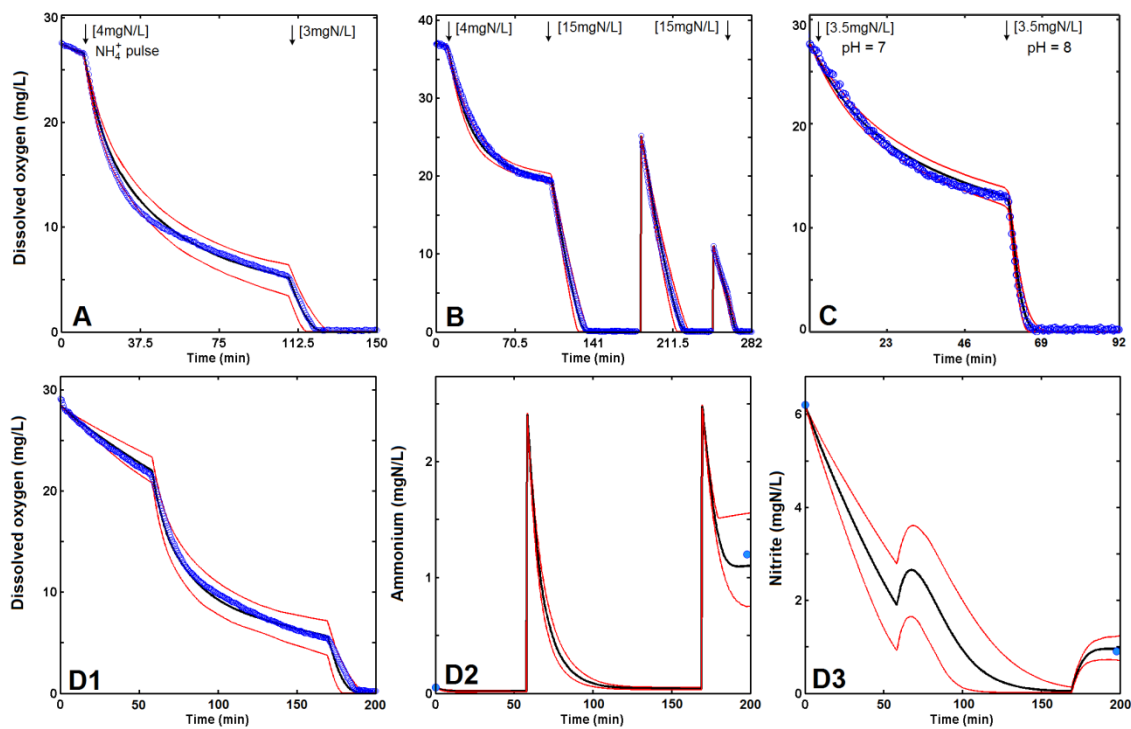


Figure 4 – Experimental DO, NH_4^+ and NO_2^- (blue markers) and model predictions (black line best-fit, red lines 95% CI). Datasets from Scen_AMO, calibration: A and B; validation: C and D.

The fitted model was evaluated on five additional experiments not used during calibration with varying initial pH (7-8), NO_2^- (0-6.2mgN/L) and NH_4^+ pulses (1-10mgN/L). The Janus coefficient and R^2 were close to unity (1.24 and 0.997) indicating a good model validation (Figure 4, C, D). In sum, the respirometric experimental design can be used to precisely identify and calibrate the primary substrate dynamics of the NDHA model based on the DO profiles.

3.2. Dynamics of N_2O during different scenarios

In the same scenarios considered for DO calibration liquid N_2O was also continuously measured (Figure 2). Moreover, the role of the primary N-substrates (NH_4^+ , NH_2OH , NO_2^- , and NO_3^-) on N_2O production was also studied under anoxic conditions (Table 1). Under conditions heterotrophic denitrification (Scen_An_HB) the presence of NO_2^- and NO_3^- did not show any net N_2O production (data not shown). However, N_2O was consumed when no other substrate was present, indicating a positive HD contribution to the total N_2O pool (Figure 5).

NOB-driven N_2O production was not detected during aerobic NO_2^- oxidation (Figure 2, left) or at the onset of anoxia in the presence of NO_2^- and NO_3^- .

AOB-driven NH_4^+ oxidation (Scen_AMO) produced a small amount of N_2O under aerobic conditions and significantly increased at the onset of anoxia (Figure 2). The specific N_2O production rate (mg N_2O -N/gVSS.min) obtained in duplicate experiments – carried out at varying biomass concentrations – were in close agreement, thus indicating biologically-driven N_2O production (SI-S6).

The role of NH_2OH as a direct precursor of N_2O was investigated in Scen_HAO. Under aerobic conditions, NH_2OH oxidation produced more N_2O than NH_4^+ oxidation. In addition, upon reaching anoxia the N_2O production rate also increased in the presence of NH_2OH (Figure 2, middle). Under anoxic conditions (Scen_An_AOB) neither NH_4^+ nor NO_2^- produced N_2O individually (SI-S6). The spike of NH_2OH yielded the largest amount of N_2O specific to the amount of nitrogen spiked, and NO_2^- was not detected at the end of the experiment ($\text{NO}_2^- < 0.05$ mgN/L). Hence, NH_2OH oxidation by AOB produces N_2O and does not require O_2 . The addition of an electron acceptor like NO_2^- to ongoing anoxic NH_2OH oxidation increased the net N_2O production rate, while addition of an electron donor as NH_4^+ did not (SI-S6).

Taken together, the N_2O production observed in all the scenarios can only be effectively predicted using the NDHA model compared to other N_2O models (Ding et al., 2016; Domingo-Félez and Smets, 2016; Ni et al., 2014; Pocquet et al., 2016).

3.2.1. Parameter estimation from N₂O dynamics

In the absence of stripping, heterotrophic denitrification is the only N₂O consuming process. First, the N₂O consumption potential of the biomass was estimated and the reduction factor was considered representative for the 4-step heterotrophic denitrification processes ($\eta_{HD} = 0.055$) (Figure 5, A). Then, N₂O production observed from NH₄⁺ oxidation at high DO, where the interference of the two denitrifying pathways is minimum, was used to calibrate the NN pathway. ϵ_{AOB} , the most sensitive parameter at high DO was calibrated, $\epsilon_{AOB} = 0.00048$ (Figure 5, B, SI-S2). Experiments from Scen_AMO were designed to reach anoxia at varying HNO₂ concentrations (0.15-3 $\mu\text{gN/L}$). Parameters associated to the ND pathway were the most sensitive and were thus calibrated ($\eta_{NOR} = 0.16$, $K_{AOB.HNO_2} = 0.67 \mu\text{gN/L}$, $K_{NH_2OH.ND} = 0.25 \text{ mgN/L}$) (SI-S2, S7). The abiotic contribution measured was low and not considered during parameter estimation (SI-S6).

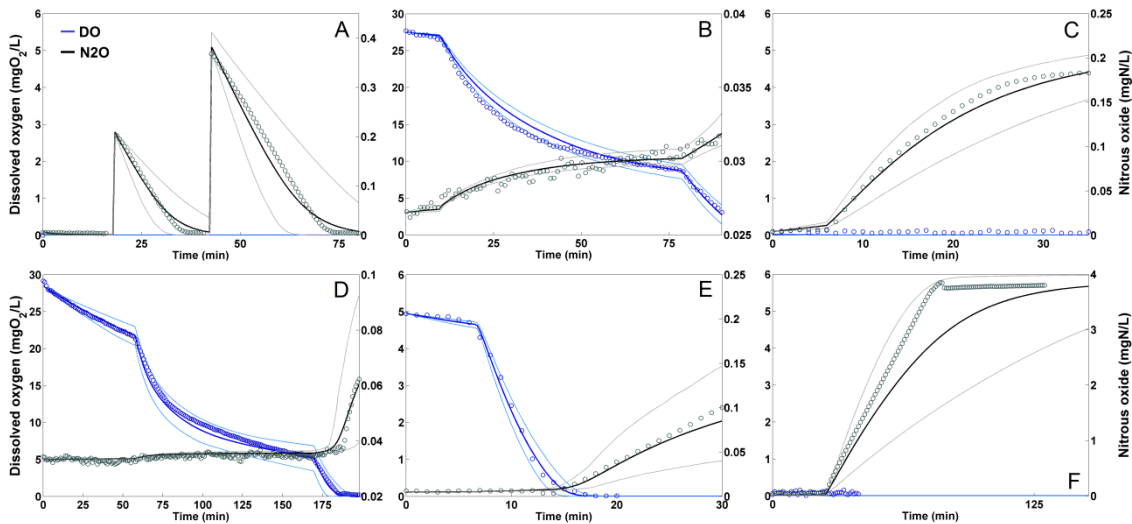


Figure 5 – Experimental N₂O (blue markers) and model predictions (dark line best-fit, light lines 95% CI) for the N₂O calibration. Datasets from calibration: (A) Scen_An_HB (N₂O pulse), (B) Scen_AMO (Aerobic NH₄⁺ pulse), (C) Scen_An_AOB (Anoxic NH₂OH pulse). Datasets from validation: (D, E) Scen_AMO (Aerobic → anoxic NH₄⁺ pulse), (F) Scen_An_AOB (NH₂OH pulse).

Validation of model response and secondary substrate (N₂O) parameter estimates

The calibrated NDHA model described the N₂O production dynamics and yield observed in the calibration datasets (F-test = 1). In all but one of the assays randomness was the most important part of the error based on the MSE analysis (SI-S5). After calibration the ARIL narrowed by 58% from the original resolution and the PUCI increased by 71% (n = 6 assays).

The predictive ability of the model was evaluated on three batches with lower HNO₂ and with higher NH₂OH pulses (HNO₂ < 0.15 $\mu\text{gN/L}$, NH₂OH = 2 mgN/L). The average Janus coefficient of the validation prediction was 1.57 and R² was 0.985, indicating a good validation

(Figure 5, D, E, F). Hence, the NDHA model could describe the N_2O production rates at a range of DO and HNO_2 concentrations.

The simple experimental design allowed the isolation of the various components of N_2O dynamics during NH_4^+ oxidation, and the parameter estimation procedure the identification of relevant model parameters.

3.3. Model predictions under varying DO and HNO_2 : Scenario analysis

To investigate the effect of DO and HNO_2 on N_2O production the NDHA model was evaluated at varying DO and HNO_2 concentrations at $pH = 7.5$ (Figure 6) with the newly estimated parameters. The model predicted the largest N_2O emission at the lowest DO and high HNO_2 (> 20%, SI-S8); and the lowest N_2O emission at the highest DO and lowest HNO_2 (0.13%). The effect of increasing HNO_2 is seen at every DO level ($DO_{0.3}$: 0.33 \rightarrow 5.4%, $DO_{5.0}$: 0.13 \rightarrow 0.28%). Conversely, increasing DO lowered the N_2O emission factor regardless of the HNO_2 level. The NO emission showed an increasing pattern with HNO_2 but a minimum was found at $DO = 2.0$ mg/L, further increasing at higher DO (SI-S8).

The contribution of the NN pathway was maximum when HNO_2 was not present and decreased with increasing HNO_2 , at a faster rate at lower than at higher DO (2.4 and 47% respectively). The ND contribution followed opposite trends, indicating a shift between autotrophic pathways driven by HNO_2 and DO. The ND contribution increased with HNO_2 , at a steeper rate at lower DO (97.4%) than at higher (53%). The HD contribution was maximum at low DO and high HNO_2 but only reached 0.2% (SI-S8).

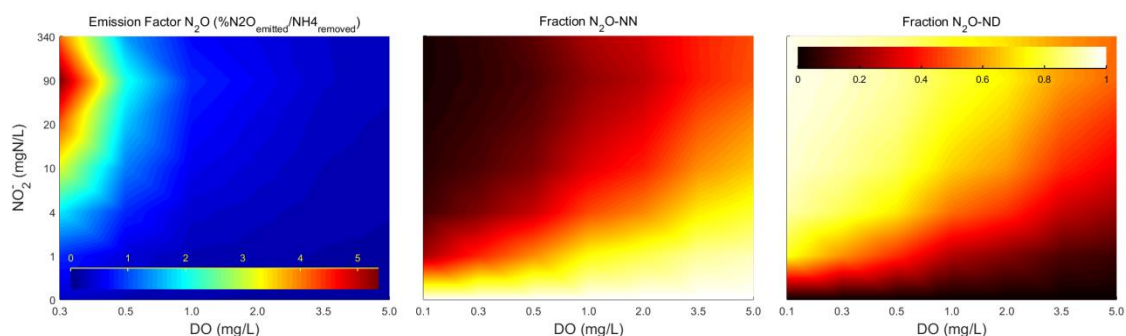


Figure 6 – Scenario analysis using the validated NHDA simulation model. Simulations were run under constant DO levels (0.1 - 0.3 - 0.5 - 1.0 - 2.0 - 3.5 - 5.0 mg/L), NO_2^- (0 – 1 – 4 – 10 – 20 – 90 – 340 mgN/L). (Left) N_2O emission factor ($\% N_2O/NH_4^+$), colorbar: 0 – 5%, blue - red. (Middle, Right) NN, ND Pathway contribution (-), colorbar: 0 – 1, black - white.

4. Discussion

4.1. Parameter estimation from respirometric assays: oxygen consumption

The respirometric experiments were used to investigate the oxygen-consuming processes driven by the AOB-enriched biomass in the presence of reduced N-species (NH_4^+ , NH_2OH and NO_2^-). If a model captures accurately the relevant oxygen-consuming processes, then DO and the primary N-substrates are predicted accurately. The experimental design based on the concatenated oxygen consumption allowed the isolation of individual processes independently (endogenous $\rightarrow \text{NO}_2^- \rightarrow \text{NH}_4^+$) (Chandran and Smets, 2005).

The calibrated model could describe the endogenous oxygen uptake and NO_2^- oxidation in Scen_NOB. However, because of the low NOB abundance the oxygen consumption from NO_2^- oxidation was low, shown by a similar sensitivity of NOB and endogenous parameters to oxygen consumption after NO_2^- spikes (Figure 3).

In Scen_AMO oxygen consumption was very sensitive to NH_4^+ dynamics (SI-S2), which yielded precise estimates for $\mu_{\text{AOB.AMO}}$, $K_{\text{AOB.NH}_3}$ and $K_{\text{AOB.O}_2.\text{AMO}}$ (Table 2). The maximum AOB growth rate ($\mu_{\text{AOB.AMO}} = 0.49$ 1/d) is in the low range of literature values found for *N. europaea* (0.56-1.62 1/d) (Brockmann et al., 2008). The biomass concentration (X_{AOB}), growth yield (Y_{AOB}) and maximum growth rate cannot be simultaneously identified from short experiments solely with DO data (Ellis et al., 1996; Petersen et al., 2001). Hence, the estimated growth rate is linearly dependent on the fixed values for X_{AOB} and Y_{AOB} : a lower initial condition for X_{AOB} would yield a higher estimate for $\mu_{\text{AOB.AMO}}$. Overall, the maximum specific NH_4^+ oxidation, $7.54 \pm 0.1 \text{E-}05$ gN/gVSS_(AOB)/h, was similar to other literature values for an AOB-enriched biomass (Ciudad et al., 2006). For the same NH_4^+ concentration, the higher oxygen consumption rate observed at higher pH was predicted by considering NH_3 the true substrate. The estimated affinities for both NH_4^+ oxidation substrates ($K_{\text{AOB.NH}_3} = 0.12$ mgN/L, $K_{\text{AOB.O}_2.\text{AMO}} = 0.23$ mg/L) were in range of literature values (Magrı et al., 2007; Park and Noguera, 2007).

Overall, the precision of the identified parameter was high (CV < 7%), common from respirometric studies (Petersen et al., 2001). It should be noted that the concentration of the spikes did not include uncertainty and was not estimated, which decreased the uncertainty of model predictions (Gernaey et al., 2002).

4.2. Role of NH_4^+ oxidation intermediates on N_2O production: experimental and modelling results

Nitrification plays an important role on N_2O emissions from N-removing systems, where NH_4^+ , NO_2^- and DO are the main substrates. Experimental results indicated that aerobic NH_4^+ -oxidation products, NH_2OH and NO_2^- were responsible for the higher N_2O production rate at the

onset of anoxia and not NH_4^+ itself, which requires molecular O_2 for its oxidation (Sayavedra-Soto et al., 1996) (SI-S6). NH_2OH has been shown to be a key compound regulating N_2O production by AOB (Caranto et al., 2016; de Bruijn et al., 1995; Kozłowski et al., 2016). Because of its high reactivity under aerobic and anoxic conditions, it is an important electron donor for the cytochrome pool of AOB. Previous studies have shown the higher N_2O yield of nitrifying biomass and pure cultures fed on NH_2OH compared to NH_4^+ , also observed in Scen_HAO ($\text{N}_2\text{O_R}_{\text{NH}_2\text{OH}}/\text{N}_2\text{O_R}_{\text{NH}_4^+} = 40$) (Figure 2) (Kim et al., 2010; Kozłowski et al., 2016). Here we show that even under anoxic conditions the sole presence of NH_2OH also yields a large amount of N_2O (SI-S6), recently suggested as a new N_2O producing pathway by (cyt) P460 (Caranto et al., 2016). The addition of an electron donor like NO_2^- further increased N_2O production, highlighting the role of the primary N-substrates on N_2O dynamics, especially of NH_2OH .

The NDHA model captures the observed anoxic NH_2OH oxidation to N_2O with no HNO_2 production associated. A NH_2OH pulse in the concentration range of reported measurements (0.1mgN/L) could be described in the calibration dataset (Figure 5, F-test = 1, $R^2 > 0.99$); and at higher NH_2OH concentrations (2 mgN/L) the model predicted the N_2O trend but not as accurately (Figure 5, F-test = 0, $R^2 = 0.97$). Based on the model structure of other two-pathway models for AOB none can predict the observed N_2O dynamics. In certain models NH_2OH does not react under anoxic conditions (Ding et al., 2016; Pocquet et al., 2016), or reacts producing both N_2O and HNO_2 (Ni et al., 2014).

Under a variety of DO, HNO_2 and NH_3 concentrations the calibrated NDHA model could describe the observed N_2O dynamics. Other models, with varying degrees of complexity, have also described the effect of HNO_2 and DO (4-6 processes) but the effect of NH_2OH , the main driver of N_2O production, was not considered (Ding et al., 2016; Ni et al., 2014). The scenario analysis indicated a shift between the main pathway contributions governed by DO and HNO_2 (Figure 6). This relationship has been described by other two-pathway models, where ND was the main contributor to the N_2O emission factor during NH_4^+ oxidation and the highest N_2O emission factor was observed at low DO (Ni et al., 2014; Pocquet et al., 2016).

4.3. N_2O model calibration

4.3.1. Analysis of the NDHA parameter estimates.

In the last years new N_2O models have improved their best-fit predictions under different scenarios (i.e. varying DO, NO_2^-) by increasing the number of processes and variables considered. For example, all the models describe the ND pathway with a NO_2^- dependency (Ni et al., 2011; Pocquet et al., 2016; Schreiber et al., 2009), or the NN pathway as a fraction of the

NH_2OH oxidation to NO_2^- (Ni et al., 2014; Pocquet et al., 2016). While the intermediates of NH_4^+ oxidation or the process rates are described differently, some parameters are common across N_2O models.

In this study, the contribution of the NN pathway ($\epsilon_{\text{AOB}} = 0.048\% \mu_{\text{AOB.HAO}}$) is in the low range of other reported values (0.052-0.15%), while the maximum N_2O production rate, described by $\eta_{\text{NOR}} = 0.16$, lies in the range (0.07 – 0.34). In agreement with the ND description of the model by Pocquet et al., (2016), the electron acceptor of the ND pathway was HNO_2 instead of NO_2^- . Increasing N_2O production rates were observed at higher HNO_2 but constant NO_2^- (9.5-10mgN/L, 0.8-1.5 $\mu\text{gHNO}_2\text{-N/L}$). The affinity for HNO_2 ($K_{\text{AOB.HNO}_2} = 0.67 \mu\text{gHNO}_2\text{-N/L}$, 17.1 mg NO_2^- -N/L, pH 7.5, 20 °C) could be estimated from experiments run at varying HNO_2 (0.16-1.5 $\mu\text{gHNO}_2\text{-N/L}$). The affinity for NO_2^- is 100 times lower than other nitrifying systems, but 15 times higher than a NO_2^- -accumulating biomass ($K_{\text{AOB.NO}_2^-} = 0.14$, 282 mgN/L)(Pocquet et al., 2016; Schreiber et al., 2009). The difference could be explained by the operating conditions at which each biomass is acclimated: low NO_2^- for activated sludge systems ($\approx 0.5\text{mgN/L}$) and high NO_2^- for nitrating reactors (50-150 mg NO_2^- -N/L in the parent reactor of this study). The NDHA model combined with the experimental design allows the simultaneous estimation of parameters describing main N-substrates and N_2O dynamics from simple respirometric experiments.

4.3.2. N_2O models: response validation and identifiability

As N_2O models produce better fits discrimination tools become more important. If the capabilities of two models to describe dynamic N_2O trends are similar (Lang et al., 2017; Pan et al., 2015) visual inspection or metrics such as R^2 are not sufficient, and more rigorous statistics as the F-test used in this study are necessary for model discrimination.

The parameter subset selection during calibration of each scenario was based on the lower AIC criteria. The identifiability of the estimated parameters was assessed by the correlation matrix and the precision of the estimated parameters ($\text{CV} < 5\%$). The triplet $K_{\text{AOB.HNO}_2}$, $K_{\text{AOB.NH}_2\text{OH.ND}}$ and η_{NOR} were estimated with the same dataset, and based on their collinearity index ($\gamma > 15$) they are not identifiable and their values depend on the others. This metric is based on local sensitivities, and as shown in (Table 2), the high correlation between $K_{\text{AOB.NH}_2\text{OH.ND}}$ and η_{NOR} could be responsible for the high collinearity of the triplet. An improved experimental design or an additional dataset such as NO would improve the identifiability these parameters, as shown for other two-pathway N_2O models (Pocquet et al., 2016). Together with the best-fit prediction the 95% CI of the calibrated NDHA model bracketed the experimental datasets, validating the model response.

The uncertainty of estimates (CV, correlation matrix) is not always reported in literature (Ding et al., 2016; Kim et al., 2017; Spérandio et al., 2016), which hampers critical discrimination procedures. While some models have reported the estimated variance identifiability metrics are scarce and not assessed. To the authors knowledge none of the proposed N₂O models has studied how the uncertainty of parameter estimates affects N₂O predictions (e.g. ARIL, PUCI). Moreover, the analysis of residuals shows that high frequency data such as online sensors can lead to autocorrelated residuals in N₂O measurements (SI-S5). While very high precision of estimates is possible, testing the model response can avoid a possible over interpretation of the dataset and uncertainty underestimation (CV \ll 0.001% (Peng et al., 2015)). In this study we show that addressing parameter identifiability after model calibration will benefit N₂O model discrimination studies.

4.4. N₂O model uncertainty

With the final objective of designing N₂O mitigation strategies, the confidence of model predictions is critical when quantifying N₂O emissions. As a by-product of NH₄⁺ oxidation, the uncertainty associated to NH₄⁺ removal processes will propagate to N₂O predictions. The respirometric experimental design allowed for accurate estimates and narrow 95% confidence intervals for DO, NH₄⁺ and other N-species, which was critical to reduce the predicted uncertainty for N₂O (SI-S9). N₂O models have been calibrated by sequentially fitting the primary N-substrates followed by the N₂O dynamics (Ni et al., 2014; Pocquet et al., 2016). The effect of propagating the uncertainty from the calibration of primary N-substrates to N₂O was not discussed. Consequently, the precision of the N₂O calibration could be overestimated.

To evaluate the performance of the parameter estimation results N₂O emissions from a simulated case study were examined via Monte-Carlo simulations (pH = 7.5, NH₄⁺ = 70 mgN/L, DO = 0.3, 1.3 mg/L and NO₂⁻ = 0, 1, 5, 15, 100 mgN/L, 500 simulations). At pseudo-steady state the standard error of the Monte-Carlo simulations shows the propagated uncertainty. For the 10 parameters estimated in this study the normalized uncertainty associated to their default class (Sin et al., 2009) is approximately 40% of the N₂O emission factor (Figure 7). If the calibration results from this experimental design are considered instead (Table 2), the uncertainty decreases to 10% (Figure 7). These results highlight the importance of considering uncertainty propagation in N₂O predictions, as N₂O emissions are greatly affected by the uncertainty of primary N-substrates.

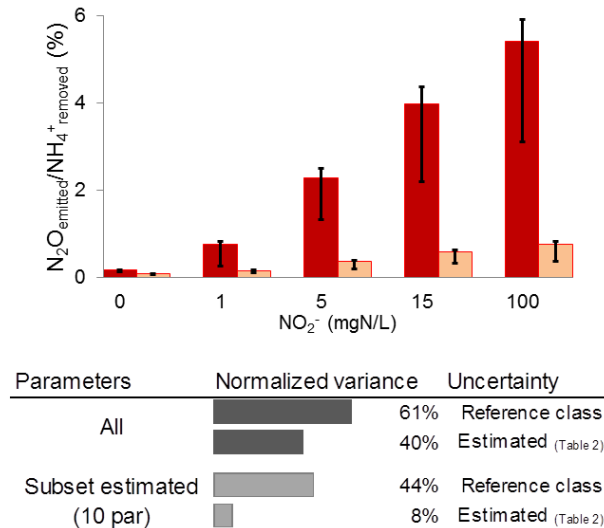


Figure 7 – Model evaluation results (500 runs) at pseudo-steady state for NH_4^+ removal at constant DO and NO_2^- : AOB-enriched biomass, $\text{pH} = 7.5$, $\text{NH}_4^+ = 70$ mgN/L, DO ([0.3 – 1.3] mg/L) and NO_2^- [0 – 1 – 5 – 15 – 100] mgN/L. (Top) N_2O emission factor at low DO (red) and high DO (light red); top standard error corresponds to uncertainty of estimated parameters only (Table 2), bottom standard error corresponds to uncertainty in All model parameters. (Bottom) Normalized variance for uncertainty considered in All model parameters (dark grey) or only for the 10 parameters estimated in this study (light grey) (Table 2) with default uncertainty (top bar) or from this study (Table 2) (bottom bar).

Conclusions

- A novel experimental design to calibrate N_2O models through extant respirometry is proposed that combines DO and N_2O measurements.
- Parameters associated to NO_2^- and NH_4^+ oxidation were sequentially fitted to DO consumption profiles by isolating individual processes. Five parameters were identified from the DO dataset and another five were estimated from the N_2O dataset with low uncertainty ($\text{CV} < 10\%$).
- The NDHA model response was validated and described AOB-driven N_2O production at varying DO and HNO_2 concentrations.
- For the first time the uncertainty of the calibrated parameters was propagated to the model outputs in a simulation case study, and compared to the uncertainty from a reference case. The uncertainty of the N_2O emission factor predicted was reduced from $\sim 40\%$ of its value to $\sim 10\%$.

Software availability

The MATLAB/SIMULINK code containing the implementation of the model is free upon request to the corresponding author.

Acknowledgements

This research was funded by the Danish Agency for Science, Technology and Innovation through the Research Project LaGas (12-132633). The authors have no conflict of interest to declare.

References

- Akaike, H., 1974. A new look at the statistical model identification. *IEEE Trans. Automat. Contr.* 19, 716–723. doi:10.1109/TAC.1974.1100705
- Beale, E.M.L., 1960. Confidence Regions in Non-Linear Estimation. *J. R. Stat. Soc. Ser. B-statistical Methodol.* 22, 41–88. doi:10.2307/2983877
- Bennett, N.D., Croke, B.F.W., Guariso, G., Guillaume, J.H.A., Hamilton, S.H., Jakeman, A.J., Marsili-Libelli, S., Newham, L.T.H., Norton, J.P., Perrin, C., Pierce, S.A., Robson, B., Seppelt, R., Voinov, A.A., Fath, B.D., Andreassian, V., 2013. Characterising performance of environmental models. *Environ. Model. Softw.* 40, 1–20. doi:10.1016/j.envsoft.2012.09.011
- Brockmann, D., Rosenwinkel, K.-H., Morgenroth, E., 2008. Practical identifiability of biokinetic parameters of a model describing two-step nitrification in biofilms. *Biotechnol. Bioeng.* 101, 497–514. doi:10.1002/bit.21932
- Brouwer, H., Klapwijk, A., Keesman, K.J., 1998. Identification of activated sludge and wastewater characteristics using respirometric batch-experiments. *Water Res.* 32, 1240–1254. doi:10.1016/S0043-1354(97)00334-5
- Brun, R., Kühni, M., Siegrist, H., Gujer, W., Reichert, P., 2002. Practical identifiability of ASM2d parameters--systematic selection and tuning of parameter subsets. *Water Res.* 36, 4113–27.
- Brun, R., Reichert, P., Kfinsch, H.R., 2001. Practical identifiability analysis of large environmental simulation models. *Water Resour. Res.* 37, 1015–1030.
- Campolongo, F., Saltelli, A., 1997. Sensitivity analysis of an environmental model: an application of different analysis methods. *Reliab. Eng. Syst. Saf.* 57, 49–69. doi:10.1016/S0951-8320(97)00021-5
- Caranto, J.D., Vibert, A.C., Lancaster, K.M., 2016. Nitrosomonas europaea cytochrome P460 is a direct link between nitrification and nitrous oxide emission. *Proc. Natl. Acad. Sci.* 113, 14704–14709. doi:10.1073/pnas.1611051113
- Castro-Barros, C., Rodríguez-Caballero, A., Volcke, E.I.P., Pijuan, M., 2016. Effect of nitrite on the N₂O and NO production on the nitrification of low-strength ammonium wastewater. *Chem. Eng. J.* 287, 269–276. doi:10.1016/j.cej.2015.10.121
- Chandran, K., Hu, Z., Smets, B.F., 2008. A critical comparison of extant batch respirometric and substrate depletion assays for estimation of nitrification biokinetics. *Biotechnol. Bioeng.* 101, 62–72. doi:10.1002/bit.21871
- Chandran, K., Smets, B.F., 2005. Optimizing experimental design to estimate ammonia and nitrite oxidation biokinetic parameters from batch respirograms. *Water Res.* 39, 4969–78. doi:10.1016/j.watres.2005.10.001
- Cierkens, K., Plano, S., Benedetti, L., Weijers, S., de Jonge, J., Nopens, I., 2012. Impact of influent data frequency and model structure on the quality of WWTP model calibration and uncertainty. *Water Sci. Technol.* 65, 233–42. doi:10.2166/wst.2012.081
- Ciudad, G., Werner, A., Bornhardt, C., Muñoz, C., Antileo, C., 2006. Differential kinetics of ammonia- and nitrite-oxidizing bacteria: A simple kinetic study based on oxygen affinity and proton release during nitrification. *Process Biochem.* 41, 1764–1772. doi:10.1016/j.procbio.2006.03.032
- de Bruijn, P., van de Graaf, A.A., Jetten, M.S.M., Robertson, L.A., Kuenen, J.G., 1995. Growth of Nitrosomonas europaea on hydroxylamine. *FEMS Microbiol. Lett.* 125, 179–184.
- Ding, X., Zhao, J., Hu, B., Chen, Y., Ge, G., Li, X., Wang, S., Gao, K., Tian, X., 2016. Mathematical modeling of nitrous oxide production in an anaerobic/oxic/anoxic process. *Bioresour. Technol.* 222, 39–48. doi:10.1016/j.biortech.2016.09.092

- Dochain, D., Vanrolleghem, P.A., 2001. *Dynamic Modelling and Estimation in Wastewater Treatment Processes*. IWA Publishing, London, UK.
- Domingo-Félez, C., Pellicer-Nàcher, C., Petersen, M.S., Jensen, M.M., Plósz, B.G., Smets, B.F., 2017. Heterotrophs are key contributors to nitrous oxide production in activated sludge under low C-to-N ratios during nitrification-Batch experiments and modeling. *Biotechnol. Bioeng.* 114, 132–140. doi:10.1002/bit.26062
- Domingo-Félez, C., Smets, B.F., 2016. A consilience model to describe N₂O production during biological N removal. *Environ. Sci. Water Res. Technol.* 2, 923–930. doi:10.1039/C6EW00179C
- Ellis, T.G., Barbeau, D.S., Smets, B.F., Grady, C.P.L., 1996. Respirometric technique for determination of extant kinetic parameters describing biodegradation. *Water Environ. Res.* 68, 917–926. doi:10.2175/106143096X127929
- Gernaey, K., Petersen, B., Dochain, D., Vanrolleghem, P.A., 2002. Modeling aerobic carbon source degradation processes using titrimetric data and combined respirometric-titrimetric data: structural and practical identifiability. *Biotechnol. Bioeng.* 79, 754–67. doi:10.1002/bit.10337
- Graaf, A.A. Van De, Bruijn, P. De, Robertson, L.A., Jetten, M.S.M., Kuenen, J.G., 1996. Autotrophic growth of anaerobic ammonium-oxidizing microorganisms in a fluidized bed reactor. *Microbiology* 142, 2187–2196.
- Guo, L., Vanrolleghem, P. a., 2014. Calibration and validation of an activated sludge model for greenhouse gases no. 1 (ASMG1): prediction of temperature-dependent N₂O emission dynamics. *Bioprocess Biosyst. Eng.* 37, 151–163. doi:10.1007/s00449-013-0978-3
- Gustavsson, D.J.I., Tumlin, S., 2013. Carbon footprints of Scandinavian wastewater treatment plants. *Water Sci. Technol.* 68, 887. doi:10.2166/wst.2013.318
- Haefner, J.W., 2005. *Modeling Biological Systems: Principles and Applications*, Second. ed. Springer.
- Hiatt, W.C., Grady, C.P.L., 2008. An updated process model for carbon oxidation, nitrification, and denitrification. *Water Environ. Res.* 80, 2145–2156. doi:10.2175/106143008X304776
- Igarashi, N., Moriyama, H., Fujiwara, T., Fukumuri, Y., Tanaka, N., 1997. The structure of hydroxylamine oxidoreductase from a nitrifying chemoautotrophic bacterium, *Nitrosomonas europaea*. *Nature* 4, 276–284.
- Jin, X., Xu, C.-Y., Zhang, Q., Singh, V.P., 2010. Parameter and modeling uncertainty simulated by GLUE and a formal Bayesian method for a conceptual hydrological model. *J. Hydrol.* 383, 147–155. doi:10.1016/j.jhydrol.2009.12.028
- Kampschreur, M.J., van der Star, W.R.L., Wienders, H.A., Mulder, J.W., Jetten, M.S.M., van Loosdrecht, M.C.M., 2008. Dynamics of nitric oxide and nitrous oxide emission during full-scale reject water treatment. *Water Res.* 42, 812–26. doi:10.1016/j.watres.2007.08.022
- Kim, M., Wu, G., Yoo, C., 2017. Quantification of nitrous oxide (N₂O) emissions and soluble microbial product (SMP) production by a modified AOB-NOB-N₂O-SMP model. *Bioresour. Technol.* 227, 227–238. doi:10.1016/j.biortech.2016.11.127
- Kim, S.-W., Miyahara, M., Fushinobu, S., Wakagi, T., Shoun, H., 2010. Nitrous oxide emission from nitrifying activated sludge dependent on denitrification by ammonia-oxidizing bacteria. *Bioresour. Technol.* 101, 3958–63. doi:10.1016/j.biortech.2010.01.030
- Kozłowski, J.A., Kits, K.D., Stein, L.Y., 2016. Comparison of Nitrogen Oxide Metabolism among Diverse Ammonia-Oxidizing Bacteria. *Front. Microbiol.* 7, 1–9. doi:10.3389/fmicb.2016.01090
- Kozłowski, J. a, Price, J., Stein, L.Y., 2014. Revision of N₂O-producing pathways in the ammonia-oxidizing bacterium *Nitrosomonas europaea* ATCC 19718. *Appl. Environ. Microbiol.* 80, 4930–5. doi:10.1128/AEM.01061-14

- Lang, L., Pocquet, M., Ni, B.-J., Yuan, Z., Spérandio, M., 2017. Comparison of different two-pathway models for describing the combined effect of DO and nitrite on the nitrous oxide production by ammonia-oxidizing bacteria. *Water Sci. Technol.* 75, 491–500. doi:10.2166/wst.2016.389
- Law, Y., Lant, P., Yuan, Z., 2011. The effect of pH on N₂O production under aerobic conditions in a partial nitrification system. *Water Res.* 45, 5934–44. doi:10.1016/j.watres.2011.08.055
- Li, L., Xu, C.-Y., Xia, J., Engeland, K., Reggiani, P., 2011. Uncertainty estimates by Bayesian method with likelihood of AR (1) plus Normal model and AR (1) plus Multi-Normal model in different time-scales hydrological models. *J. Hydrol.* 406, 54–65. doi:10.1016/j.jhydrol.2011.05.052
- Lilliefors, H.W., 1967. On the Kolmogorov-Smirnov Test for Normality with Mean and Variance Unknown. *J. Am. Stat. Assoc.* 62, 399. doi:10.2307/2283970
- Machado, V.C., Tapia, G., Gabriel, D., Lafuente, J., Baeza, J.A., 2009. Systematic identifiability study based on the Fisher Information Matrix for reducing the number of parameters calibration of an activated sludge model. *Environ. Model. Softw.* 24, 1274–1284. doi:10.1016/j.envsoft.2009.05.001
- Magrí, A., Corominas, L., López, H., Campos, E., Balaguer, M., Colprim, J., Flotats, X., 2007. A Model for the Simulation of the SHARON Process: pH as a Key Factor. *Environ. Technol.* 28, 255–265. doi:10.1080/09593332808618791
- Ni, B.-J., Peng, L., Law, Y., Guo, J., Yuan, Z., 2014. Modeling of Nitrous Oxide Production by Autotrophic Ammonia-Oxidizing Bacteria with Multiple Production Pathways. *Environ. Sci. Technol.* 48, 3916–24. doi:10.1021/es405592h
- Ni, B.-J., Rusalleda, M., Pellicer-Nàcher, C., Smets, B.F., 2011. Modeling nitrous oxide production during biological nitrogen removal via nitrification and denitrification: extensions to the general ASM models. *Environ. Sci. Technol.* 45, 7768–76. doi:10.1021/es201489n
- Pan, Y., Ni, B.-J., Lu, H., Chandran, K., Richardson, D., Yuan, Z., 2015. Evaluating two concepts for the modelling of intermediates accumulation during biological denitrification in wastewater treatment. *Water Res.* 71, 21–31. doi:10.1016/j.watres.2014.12.029
- Park, H.-D., Noguera, D.R., 2007. Characterization of two ammonia-oxidizing bacteria isolated from reactors operated with low dissolved oxygen concentrations. *J. Appl. Microbiol.* 102, 1401–17. doi:10.1111/j.1365-2672.2006.03176.x
- Peng, L., Ni, B.-J., Ye, L., Yuan, Z., 2015. The combined effect of dissolved oxygen and nitrite on N₂O production by ammonia oxidizing bacteria in an enriched nitrifying sludge. *Water Res.* 73, 29–36. doi:10.1016/j.watres.2015.01.021
- Petersen, B., Gernaey, K. V., Vanrolleghem, P.A., 2001. Practical identifiability of model parameters by combined respirometric-titrimetric measurements. *Water Sci. Technol.* 43, 347–356.
- Pocquet, M., Wu, Z., Queinnec, I., Spérandio, M., 2016. A two pathway model for N₂O emissions by ammonium oxidizing bacteria supported by the NO/N₂O variation. *Water Res.* 88, 948–959. doi:10.1016/j.watres.2015.11.029
- Power, M., 1993. The predictive validation of ecological and environmental models. *Ecol. Modell.* 68, 33–50. doi:10.1016/0304-3800(93)90106-3
- Richardson, D., Felgate, H., Watmough, N., Thomson, A., Baggs, E., 2009. Mitigating release of the potent greenhouse gas N(2)O from the nitrogen cycle - could enzymic regulation hold the key? *Trends Biotechnol.* 27, 388–97. doi:10.1016/j.tibtech.2009.03.009
- Rodriguez-Caballero, A., Pijuan, M., 2013. N₂O and NO emissions from a partial nitrification sequencing batch reactor: exploring dynamics, sources and minimization mechanisms.

Water Res. 47, 3131–40. doi:10.1016/j.watres.2013.03.019

- Sayavedra-Soto, L.A., Hommes, N.G., Russell, S.A., Arp, D.J., 1996. Induction of ammonia monoxygenase and hydroxylamine oxidoreductase mRNAs by ammonium in *Nitrosomonas europaea*. *Mol. Microbiol.* 20, 541–548. doi:10.1046/j.1365-2958.1996.5391062.x
- Schreiber, F., Loeffler, B., Polerecky, L., Kuypers, M.M., de Beer, D., 2009. Mechanisms of transient nitric oxide and nitrous oxide production in a complex biofilm. *ISME J.* 3, 1301–1313. doi:10.1038/ismej.2009.55
- Schreiber, F., Wunderlin, P., Udert, K.M., Wells, G.F., 2012. Nitric oxide and nitrous oxide turnover in natural and engineered microbial communities: biological pathways, chemical reactions, and novel technologies. *Front. Microbiol.* 3, 372. doi:10.3389/fmicb.2012.00372
- Sin, G., Gernaey, K. V., Neumann, M.B., van Loosdrecht, M.C.M., Gujer, W., 2009. Uncertainty analysis in WWTP model applications: a critical discussion using an example from design. *Water Res.* 43, 2894–906. doi:10.1016/j.watres.2009.03.048
- Soler-Jofra, A., Stevens, B., Hoekstra, M., Picioreanu, C., Sorokin, D., van Loosdrecht, M.C.M., Pérez, J., 2016. Importance of abiotic hydroxylamine conversion on nitrous oxide emissions during nitrification of reject water. *Chem. Eng. J.* 287, 720–726. doi:10.1016/j.cej.2015.11.073
- Spérandio, M., Pocquet, M., Guo, L., Ni, B.-J., Vanrolleghem, P.A., Yuan, Z., 2016. Evaluation of different nitrous oxide production models with four continuous long-term wastewater treatment process data series. *Bioprocess Biosyst. Eng.* 39, 493–510. doi:10.1007/s00449-015-1532-2
- Terada, A., Lackner, S., Kristensen, K., Smets, B.F., 2010. Inoculum effects on community composition and nitrification performance of autotrophic nitrifying biofilm reactors with counter-diffusion geometry. *Environ. Microbiol.* 12, 2858–2872.
- Yu, R., Kampschreur, M.J., van Loosdrecht, M.C.M., Chandran, K., 2010. Mechanisms and specific directionality of autotrophic nitrous oxide and nitric oxide generation during transient anoxia. *Environ. Sci. Technol.* 44, 1313–9. doi:10.1021/es902794a

Supplementary Information

Title

Calibration of the NDHA model to describe N₂O dynamics from respirometric assays.

Author list

Carlos Domingo-Félez^a, María Calderó-Pascual^a, Gürkan Sin^b, Benedek G. Plósz^{a,l}, Barth F. Smets^{a*}

^aDepartment of Environmental Engineering, Technical University of Denmark, Miljøvej 115, 2800 Kgs. Lyngby, Denmark

^bDepartment of Chemical and Biochemical Engineering, Technical University of Denmark, Søtofts Plads 229, 2800 Kgs. Lyngby, Denmark

^lPresent address: Department of Chemical Engineering, University of Bath, Bath, England.

* Corresponding author:

Barth F. Smets, Phone: +45 4525 1600, Fax: +45 4593 2850, E-mail: b fsm@env.dtu.dk

S1 – Parent reactor operation

S2 – Sensitivity analysis

S3 – Parameter subset selection during calibration

S4 – Parameter estimation for aerobic NH₂OH oxidation

S5 – Parameter estimation results: Validation of model response and parameter estimates

S6 – AOB-driven N₂O production from primary N-substrates

S7 – Pathway contribution to total N₂O pool during model fitting

S8 – NDHA model evaluation

S9 – Uncertainty propagation during NH₄⁺ oxidation

S10 – NDHA model

Section S2 – Sensitivity analysis

Dynamic cumulative β^2 values for the global sensitivity analysis were calculated for every experiment (SRC method). The uncertainty was defined by classes for each model parameter following (Sin et al., 2009) (Table S2-1). Process rate equations and stoichiometry can be found in S10.

Table S2-1 – Uncertainty class definition for model parameters.

Parameter (θ_i)	Uncertainty Class
$i_{NXB}, i_{NXI}, i_{NXS}, VSS, Y_{AOB}, Y_{HB}, Y_{NOB}, K_{LaN2O}, K_{LaO2}, K_{LaNO}, f_{active}, f_{AOB}, f_{NOB}, f_{HB}, f_I,$	1 ($\pm 10\%$)
$b_{AOB}, b_{HB}, b_{NOB}, k_H, \eta_{HD}, \mu_{AOB_AMO}, \mu_{AOB_HAO}, \mu_{HB}, \mu_{HB_NAR}, \mu_{HB_NIR}, \mu_{HB_NOR}, \mu_{HB_NOS}, \mu_{NOB}, \eta_b, \eta_{h_anox}, \eta_{h_anaer},$	2 ($\pm 25\%$)
$K_{AOB_NH2OH}, K_{AOB_NH2OH_ND}, K_{AOB_NH3}, K_{AOB_NO}, K_{AOB_HNO2}, K_{AOB_O2_AMO}, K_{AOB_O2_HAO}, K_{AOB_O2_i}, K_{HB_NH4}, K_{HB_N2O}, K_{HB_NO}, K_{HB_NO2}, K_{HB_NO3}, K_{HB_O2}, K_{HB_O2_i_NAR}, K_{HB_O2_i_NIR}, K_{HB_O2_i_NOR}, K_{HB_O2_i_NOS}, K_{HB_S}, K_{HB_S_NAR}, K_{HB_S_NIR}, K_{HB_S_NOR}, K_{HB_S_NOS}, K_{NOB_HNO2}, K_{NOB_O2}, K_{NOB_i_HNO2}, K_{NOB_i_NH3}, K_{AOB_i_HNO2}, K_{AOB_i_NH3}, K_b_{O2}, K_X, \epsilon_{AOB}, \eta_{NIR}, \eta_{NOR},$	3 ($\pm 50\%$)

The regions of the dynamic SA considered were those with good regression ($R^2 > 0.7$). In specific parts of the experiment, for example during anoxic periods, the SRC method is not valid for the DO model output ($R^2 < 0.7$). These regions were thus not used during the analysis.

The empty region between the dynamic cumulative values and $\beta^2 = 1$ corresponds to the rest of parameters with very low sensitivity ($\beta^2 < 0.02$ not shown) and other parameters not considered for the analysis, and calibration: $Y_{XB}, VSS, biomass_active_fraction,$ etc.

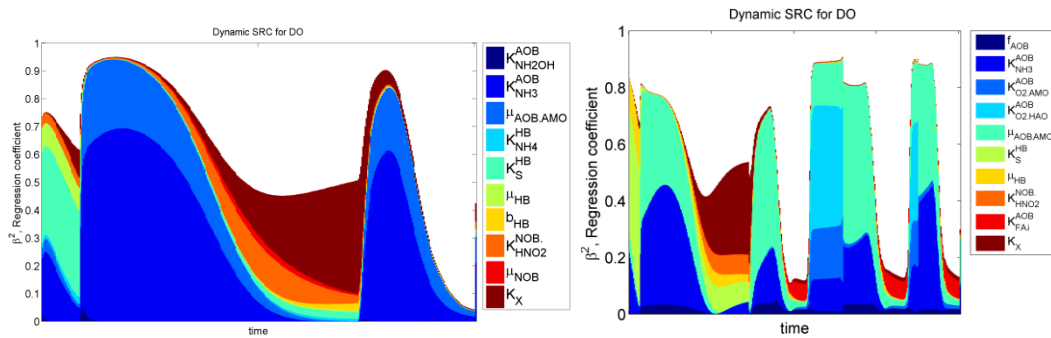


Figure S2-1 – Dynamic sensitivity analysis for DO: Scen_AMO (NH_4^+ pulses). Only parameters with squared beta (β^2) larger than 0.02 at some point of the batch are shown.

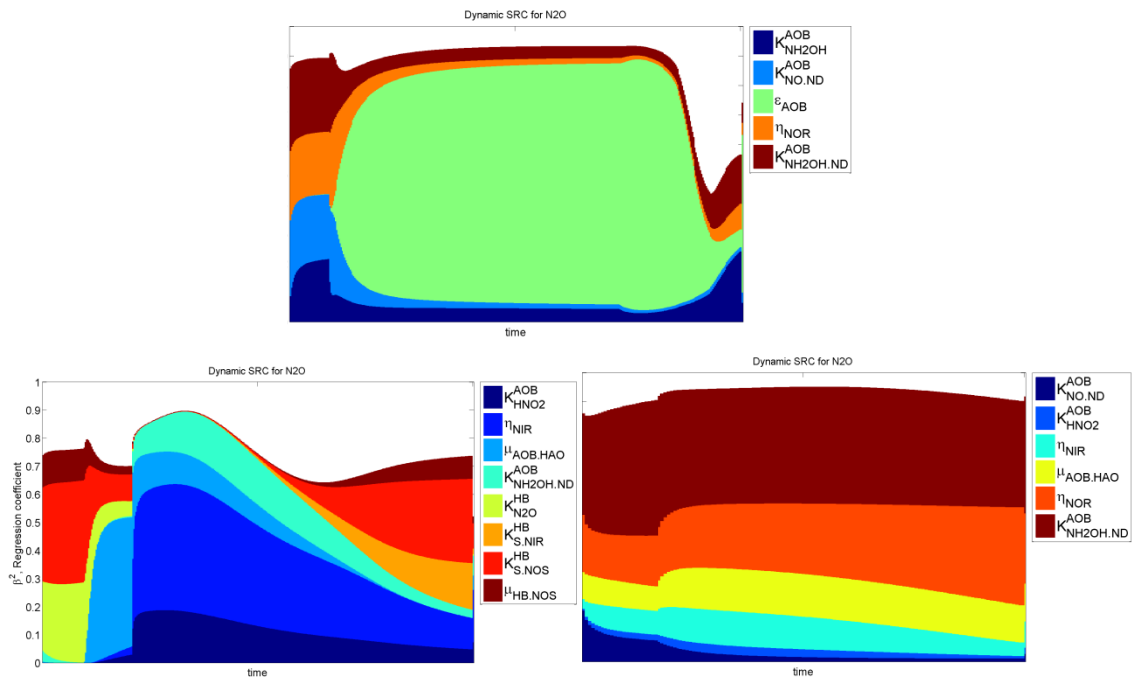


Figure S2-2 – Dynamic sensitivity analysis for N₂O: (Top) Scen_AMO (NH₄⁺ pulses). (Bottom) Scen_An_AOB (left: NH₂OH followed by NO₂⁻ pulse; right: NH₂OH pulse). Only parameters with squared beta (β²) larger than 0.02 at some point of the batch are shown.

Section S3 - Parameter subset selection during calibration

The objective of the calibration procedure was to find the minimum number of parameters that explain the scenario data with the less possible correlation amongst the subset. The same methodology was used for every scenario.

The AIC criterion aims to find the simplest model that describes the data, thus it is useful to compare subsets of different size (Akaike, 1974). The larger the RDE metric the better the capacity of a subset to explain the data with a low uncertainty in the estimates (Machado et al., 2009). The modE criterion describes the shape (relationship between largest/smallest axes) of the confidence region to prevent correlated parameters (Dochain and Vanrolleghem, 2001).

For a given size (n) all the subsets were evaluated. The best subset of size (n) was selected by the lowest AIC (blue) and largest RDE and 1/modE. Then, the subset size was increased (n+1) and all the possible subsets evaluated again. If the AIC value did not decrease for any of the new subsets the calibration was stopped in the subset with lowest AIC value (and largest RDE, 1/modE) of size (n).

Table S3-1 – Parameter subset selection procedure for Scen_NOB.

Parameters	AIC	log(RDE)	1/modE	Optimized values	Correlation	Collinearity
μ .NOB				0.00072		
K.X				0.17		
K.NOB.HNO2				0.00013		
K.HB.NH4				0.013		
k.H				0.0017		
μ .NOB / K.X				0.0008 - 0.17	0.58	3.3 - 1.4
μ .NOB / K.NOB.HNO2				0.0023 - 0.00088	0.99	35 - 24
μ .NOB / K.HB.NH4				0.0008 - 0.013	0.99	31 - 11
μ .NOB / k.H *				0.00078 - 0.0017	-0.58	3.2 - 1.4
K.X / K.NOB.HNO2				0.17 - 0.0001	-0.56	4.1 - 1.5
K.X / K.HB.NH4				0.18 - 0.0029	-0.34	3.1 - 1.5
K.X / k.H				0.22 - 0.0022	0.96	148 - 1220
K.NOB.HNO2 / K.HB.NH4				0.000019 - 0.025	-0.97	6.1 - 8.4
K.NOB.HNO2 / k.H				0.00010 - 0.0017	0.63	4.1 - 1.5
K.HB.NH4 / k.H				0.010 - 0.0017	0.61	3.5 - 1.5

(*) Parameter subset selected for calibration. Maximum rates are shown as 1/minutes.

Table S3-2 – Parameter subset selection procedure for Scen_AMO.

Parameters	AIC	log(RDE)	1/modE	Optimized values	Corrrelation	Collinearity
K.NH3				0.25		
K.O2.AMO				3.02		
μ.AMO				0.0044		
μ.HAO				0.00035		
K.X				0.173		
K.NH3 / K.O2.AMO				0.18 - 3.8	0.30	3.2-3.3
K.NH3 / μ.AMO *				0.12 - 0.0033	0.89	22.4-5.2
K.NH3 / μ.HAO				0.19 - 0.00034	-0.65	1.8-2.1
K.NH3 / K.X				0.27 - 0.098	0.76	1.9-1.9
K.O2.AMO / μ.AMO				1.6 - 0.0048	-0.91	2.5-3.7
K.O2.AMO / μ.HAO				2.0 - 0.00041	0.71	1.4-1.5
K.O2.AMO / K.X				3.5 - 0.10	-0.02	2.2-1.5
μ.AMO / μ.HAO				0.0044 - 0.0018	-0.81	2.8 - 1.0
μ.AMO / K.X				0.0043 - 0.11	-0.75	1.7-1.8
μ.HAO / K.X				0.00035 - 0.14	-0.06	1.1-1.3
K.NH3 / μ.AMO / K.O2.AMO				0.10 - 0.0031 - 0.55	0.04/-0.95/0.04	19.6-6.4
K.NH3 / μ.AMO / μ.HAO				0.10 - 0.0031 - 0.00080	-0.5/0.4/0.67	25.2-5.3
K.NH3 / μ.AMO / K.X				0.10 - 0.0031 - 0.16	-0.88/0.92/-0.94	24.5-5.4
K.NH3 / K.O2.AMO / μ.HAO				0.19 - 0.35 - 0.00033	-0.86/-0.3/0.5	2.1-2.5
K.NH3 / K.O2.AMO / K.X				0.20 - 3.6 - 0.10	-0.26/0.8/-0.46	3.9-3.5
K.NH3 / μ.HAO / K.X				0.18 - 0.00033 - 0.16	0.35/-0.4/-0.08	1.9-2.5
K.O2.AMO / μ.AMO / μ.HAO				1.6 - 0.0060 - 0.00032	-0.98/0.09/-0.16	2.6-3.6
K.O2.AMO / μ.AMO / K.X				1.6 - 0.0050 - 0.10	-0.47/0.35/-0.92	2.9-4.3
K.O2.AMO / μ.HAO / K.X				0.29 - 0.00034 - 0.15	0.76/-0.89/-0.70	1.4-2.4
μ.AMO / μ.HAO / K.X				0.0060 - 0.00032 - 0.16	-0.78/0.25/-0.62	2.0-3.0

(*) Parameter subset selected for calibration. Maximum rates are shown as 1/minutes.

Section S4 – Parameter estimation for aerobic NH₂OH oxidation

Modelling the HAO process in literature

In the past years N₂O models describing NH₄⁺ oxidation to NO₂⁻ have included NH₂OH as an obligate intermediate (Domingo-Félez and Smets, 2016; Ni et al., 2011; Ni et al., 2013a; Ni et al., 2014; Pocquet et al., 2016). Only recently the colorimetric method developed by (Frear and Burrell, 1955) has been applied to wastewater treating operations. NH₂OH is not widely monitored and results from biological NH₄⁺-removing systems have shown NH₂OH levels between 0.01-0.15 mgN/L (Table S4). However, N₂O models have not been calibrated with NH₂OH datasets but with NH₄⁺, NO₂⁻, DO and less frequently NO.

Table S4 – Reported NH₂OH measurements from biological NH₄⁺-removing systems.

Reference	NH ₂ OH (mgN/L)	System
(Soler-Jofra et al., 2016)	0.03 - 0.11	Full-scale SHARON (n = 5, Jan-Jun'15). Sampled during aeration.
(Udert et al., 2005)	< 0.14	Lab-scale membrane bioreactor, influent NH ₄ -NO ₂ (1:1).
(Harper et al., 2009)	≈ 0*	Lab-scale nitrifying bioreactor, autotrophic biomass.
(De Clippeleir et al., 2013)	< 0.2	OLAND, one-stage PNA.
(Kinh et al., 2016)	0.01 - 0.11 - 0.15	Lab-scale partial nitrification, SBR [pH 6.3 - 8.3 - 7.3]
(Yu and Chandran, 2010)	≈ 0.03, max 0.05	Batch culture exponential growth of Nitrosomonas sp.

(*) data not reported

The hydroxylamine oxidoreductase (HAO) catalyses the NH₂OH oxidation to HNO₂ with H₂O as electron acceptor and not O₂ (Hooper and Terry, 1979; Sayavedra-Soto et al., 1996). The oxidation of NH₂OH (specifically the further intermediate nitroxyl, HNO) to HNO₂ is assumed to involve O₂ because it does not occur under anoxia (Hooper and Terry, 1979). Still, the enzyme-catalysed aerobic conversion of NO to HNO₂ has not been demonstrated and the reduction of O₂ is believed to a parallel reaction occurring in cyt(aa3), a proton pumping terminal cytochrome oxidase (Figure S4-1) (Upadhyay et al., 2006). In recent N₂O models the sequential NH₂OH oxidation to NO₂⁻ via NO is described with O₂ as electron acceptor and thus anoxic NH₂OH oxidation does not occur (Ni et al., 2013a; Pocquet et al., 2016). Only the NDHA model can describe N₂O production from both aerobic and anoxic NH₂OH oxidation (with and without NO₂⁻ production).

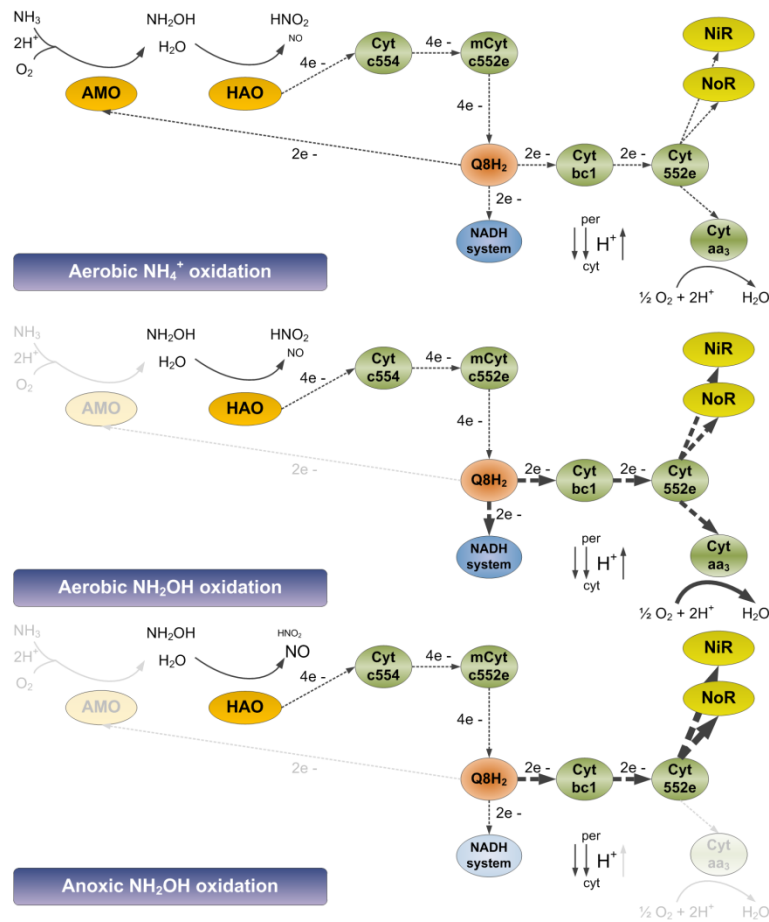


Figure S4-1 - Schematic of NH₃ oxidation to HNO₂ by AOB, main intermediates, electron flow and enzymatic sites.

Comparison of equivalent parameters from N₂O models for the AMO and HAO process show high variability. $\mu_{\text{MAX.HAO}}$ has been reported as both higher and lower than $\mu_{\text{AOB.AMO}}$, ($\mu_{\text{AOB.HAO}} / \mu_{\text{AOB.AMO}} = 0.3\text{-}2.6$ (Ni et al., 2013a)). Substrate affinity $K_{\text{NH}_2\text{OH}}$ has been assumed equal to that of NH₄⁺ or has not been targeted during calibration (Law et al., 2011; Ni et al., 2011) with values ranging from 0.7 to 2.4 mgN/L (Ding et al., 2016; Law et al., 2011; Ni et al., 2011; Pocquet et al., 2016). The oxygen affinity of the HAO process ($K_{\text{O}_2.\text{HAO}}$) has been reported at varying ratios compared to that of the AMO process ($K_{\text{O}_2.\text{HAO}}/K_{\text{O}_2.\text{AMO}} = 0.15 - 14$) (Ni et al., 2013a; Ni et al., 2013b). Overall, while four new parameters were added to the model the information content of datasets remained invariant, which lowers parameter identifiability.

The AMO process cannot be faster than the HAO as the NH₃ oxidation process requires 2 electrons supplied by NH₂OH oxidation, shown by an initial NH₄⁺ oxidation acceleration phase (Chandran and Smets, 2008; Guisasaola et al., 2006). Under steady-state, reported $K_{\text{NH}_2\text{OH}}$ together with similar $\mu_{\text{AOB.AMO}}$, $\mu_{\text{AOB.HAO}}$, $K_{\text{O}_2.\text{AMO}}$ and $K_{\text{O}_2.\text{HAO}}$ yield NH₂OH concentrations much larger than reported (≈ 1 mgN/L vs. 0.01-0.15mgN/L). The overestimation of NH₂OH concentrations does not affect the overall steady state N-balance but biased NH₂OH predictions

directly affect N_2O model calibrations because NH_2OH is direct substrate of N_2O production. The authors believe that even though describing NH_2OH oxidation is still a challenge, NH_2OH affinity should be higher than reported to predict more accurately the lower concentrations measured (Figure S4-2). N_2O model calibrations will thus benefit from more accurate NH_2OH predictions.

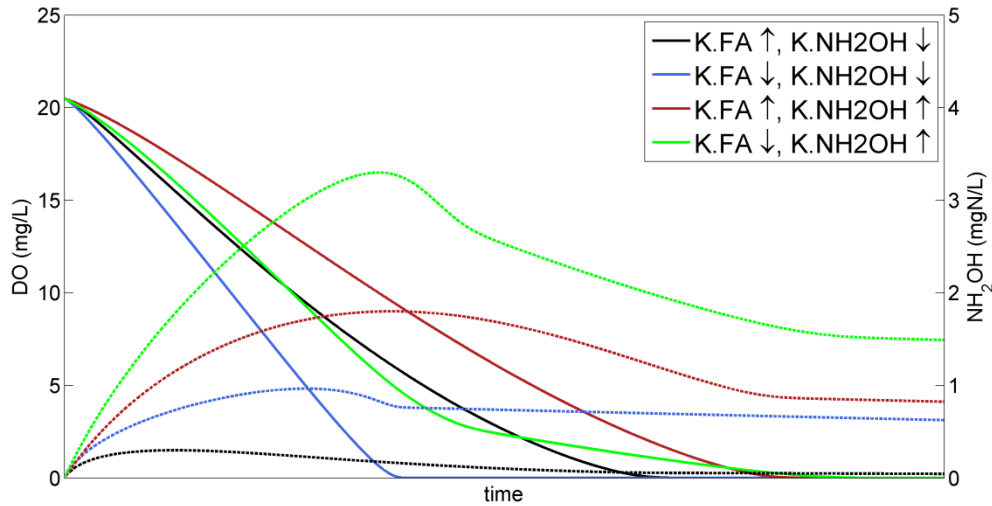


Figure S4-2 – DO model simulation for an NH_4^+ pulse ($\mu_{MAX.AMO} = \mu_{MAX.HAO}$, $K_{O_2.AMO} = K_{O_2.HAO}$, $pH = 7.5$, $25\text{ }^\circ\text{C}$) to study the effect of NH_3 and NH_2OH affinities to the DO and NH_2OH concentration profiles.

DO (straight lines), NH_2OH (dotted line). ($K_{FA-NH_3} = 0.01 - 0.1\text{ mgN/L}$, $K_{NH_2OH} = 0.2 - 2.4\text{ mgN/L}$).

Parameter estimation of Scen_HAO

To determine NH_2OH oxidation parameters independently from NH_4^+ oxidation (HAO vs. AMO) a similar approach to the 2-step nitrification procedure was used in this study (Brouwer et al., 1998). Based on the COD mass balance complete aerobic NH_2OH removal was observed (Figure S4-3, $t = 7 - 50\text{ min}$, 1.6 mgN/L consumed, approximately 2.11 mgCOD/mgN). Moreover, from the independent pH dataset a decreasing trend during NH_2OH removal agreed with the proposed reaction for the HAO process where HNO_2 is formed and mostly deprotonated at $pH \approx 7-8$ ($pK_a = 3.26$ at $25\text{ }^\circ\text{C}$). By adding NH_2OH spikes at varying DO concentrations parameters describing NH_2OH oxidation to HNO_2 in the NDHA model can be calibrated. From the sensitivity ranking the top-5 most sensitive parameters were considered for calibration: $\{\mu_{AOB.HAO}, K_{AOB.NH_2OH}, K_X, K_{AOB.NH_3}, K_{HB.NH_4}\}$ (Figure S4-3). Two parameters could be identified from this dataset: $\mu_{AOB.HAO}, K_{AOB.NH_2OH}$ (Figure S4-4).

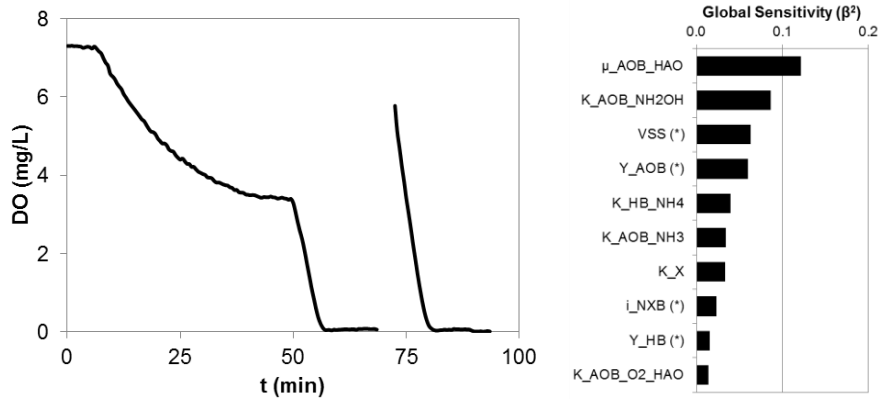


Figure S4-3 - Left: DO measurements during NH_2OH oxidation at varying NH_2OH levels (1.6mgN/L t = 7min, 4mgN/L t = 50min, 4mgN/L t = 52min, 4mgN/L at t = 75 min). Right: Corresponding DO-associated sensitivity ranking.

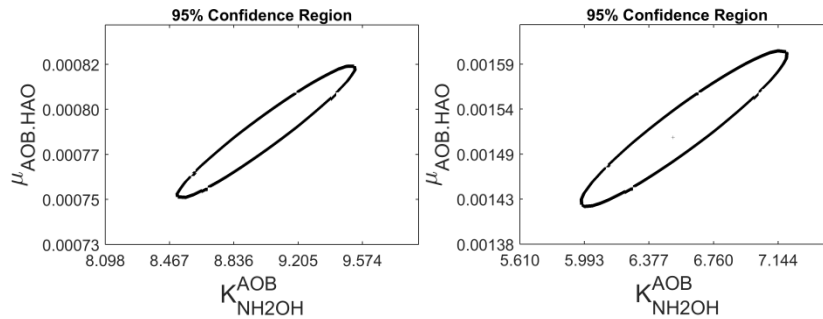


Figure S4-4 - Calibration results from Scen_HAO. Left: $K_{\text{AOB.NH}_2\text{OH}}$ and $\mu_{\text{AOB.HAO}}$ estimates for $Y_{\text{AOB}} = 0.18$ ($K_{\text{AOB.NH}_2\text{OH}} = 9.0\text{mgN/L}$, $\mu_{\text{AOB.HAO}} = 0.00078$ 1/min, CV = 2.9-2.0%, corr = 0.93, RMSE = 0.07mg/L). Right: $K_{\text{AOB.NH}_2\text{OH}}$ and $\mu_{\text{AOB.HAO}}$ estimates for $Y_{\text{AOB}} = 0.36$ assuming all 4 electrons released used for AOB growth. ($K_{\text{AOB.NH}_2\text{OH}} = 6.5\text{mgN/L}$, $\mu_{\text{AOB.HAO}} = 0.0015$ 1/min, CV = 4.8-3.0%, corr = 0.90, RMSE = 0.11mg/L).

The model described the DO profile with a low RMSE = 0.07mg/L and F-test = 1, indicating a good model prediction. Even though the estimated parameters showed a high correlation (≈ 0.9) the confidence intervals were not wide ($< 3\%$) and the collinearity index was lower than 10, indicating good identifiability ($\mu_{\text{AOB.HAO}} = 0.64$ 1/d, $K_{\text{AOB.NH}_2\text{OH}} = 9.0$ mgN/L). High correlation occurred due to an unexpected high value for $K_{\text{AOB.NH}_2\text{OH}}$ compared to $[\text{NH}_2\text{OH}_{\text{init}}]$, which leads to practical identifiability problems in the Monod kinetics (Holmberg, 1982). While $\mu_{\text{AOB.HAO}}$ is similar to other literature values, $K_{\text{AOB.NH}_2\text{OH}}$ was higher than those reported in N_2O models but in the same range as in a similar experimental design (4.9 mgN/L) (Chandran and Smets, 2008). For three different AOB species an approximately double growth yield on NH_2OH compared to NH_4^+ was observed by (Böttcher and Koops, 1994), as twice the electrons are available for growth. Moreover, more ATP was produced by AOA when NH_2OH was fed compared to NH_4^+ .

This modification was also considered in the calibration process but did not change the low affinity for NH_2OH ($Y_{\text{AOB}} = 0.18$ and 0.36 mgCOD/mgN, Figure S4-4).

Role of NH_2OH as intermediate of NH_4^+ oxidation by AOB

The estimated parameters for the HAO process during aerobic conditions ($\mu_{\text{MAX..HAO}}$, $K_{\text{AOB.NH}_2\text{OH}}$) overestimates NH_2OH concentrations during NH_4^+ spikes (> 1 mgN/L simulated vs. < 0.15 mgN/L in literature, Table S4). Thus, isolated aerobic NH_2OH oxidation is not representative of NH_2OH oxidation from NH_4^+ production as two of the four electrons released by NH_2OH oxidation to NO_2^- allow the O_2 reduction/ NH_4^+ oxidation of the AMO process. When NH_4^+ is not present these two electrons are not required and are thus channelled towards the cytochrome pool, which explains a much higher N_2O yield on NH_2OH compared to NH_4^+ (Figure 2) (de Bruijn et al., 1995; Cantera and Stein, 2007).

Overall, these findings show that a lower $K_{\text{AOB.NH}_2\text{OH}}$ is necessary to describe the low NH_2OH accumulation found in literature where, under steady-state, the AMO and HAO processes occur at the same rate. If NH_2OH accumulated after an NH_4^+ spike due to a slower HAO to AMO process the oxygen consumption rate would decrease from 3.43 to 2.29 mgCOD/mgN after NH_4^+ depletion. The same change in oxygen consumption occurs in NOB-limited nitrifying respirograms where NO_2^- is still present after NH_4^+ has been depleted (Chandran and Smets, 2000). Moreover, the release in high concentrations of the main electron source would be, potentially, a waste of energy for AOB.

Section S5 – Parameter estimation results: Validation of model response and parameter estimates.

Normality of error distribution

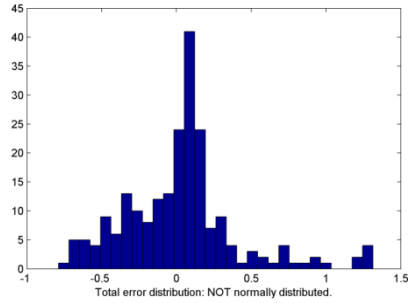


Figure S5-1. Distribution of residuals of Scen_AMO.

Data acquisition frequency impact on calibration results:

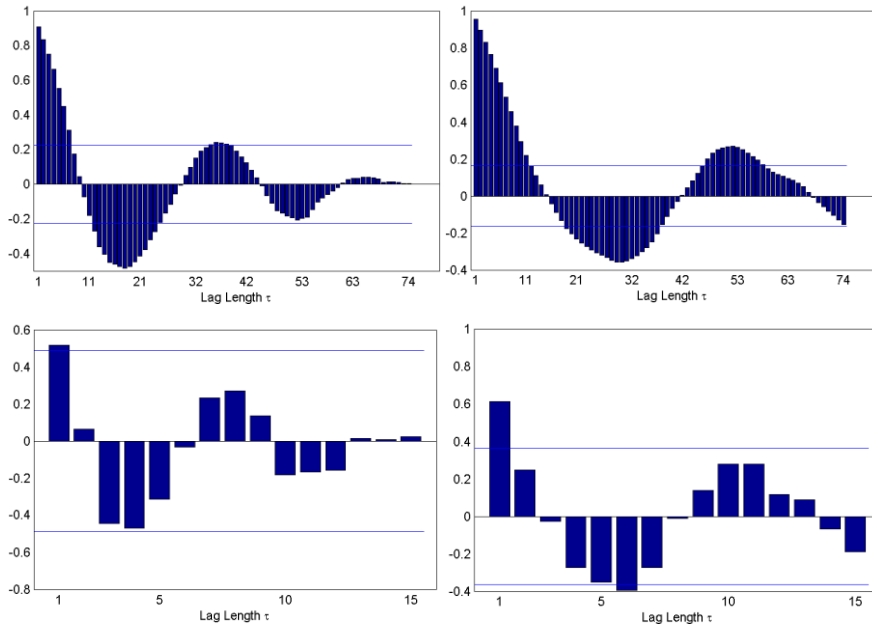


Figure S5-2. Autocorrelation function of residuals from best-fit estimates of two experiments from Scen_AMO. Data frequency = point/2min (top), point/10min (bottom).

	J_crit	Error	μ_{NOB} (1/min)	CV μ_{NOB} (%)	k_H	CV k_H (%)	Corr	F-test	Nr. points
Sampling = 0.5 min	1.01	5.95	0.000670	1.0	0.0017	0.9	-0.52	1 (2.9/3)	1020
Sampling = 2 min	1.04	5.88	0.000666	2.1	0.0017	1.8	-0.51	1 (0.8/3)	257
Sampling = 5 min	1.10	5.97	0.000669	3.4	0.0017	3.0	-0.52	1 (0.3/3)	104
Sampling = 10 min	1.20	5.74	0.000661	4.8	0.0017	4.2	-0.51	1 (0.2/3)	53

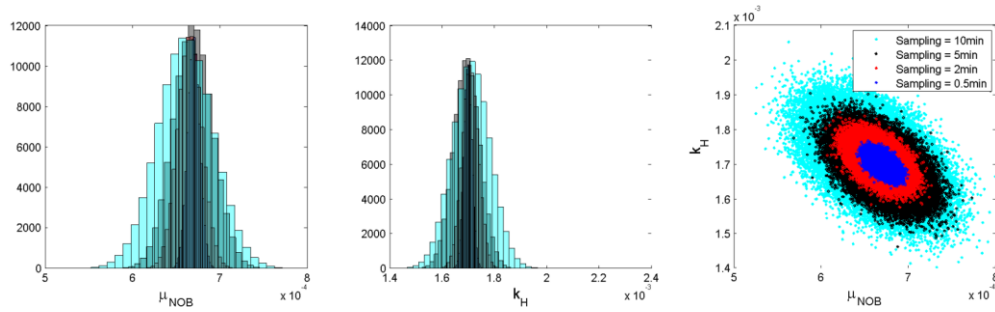


Figure S5-3. Samples from μ_{NOB} and k_H estimates for different data frequencies used for calibration (every 0.5-2-5-10 minutes).

Table S5-1 – Analysis of residuals for DO and N_2O calibration and validation.

DO calibration

Scenario	Scen_NOB			Scen_AMO			Scen_AMO_DO		
	μ_{NOB}, k_H			$\mu_{AOB, AMO}, K_{AOB, NH_3}$			$K_{AOB, O_2, AMO}$		
Parameters Estimated	Exp_1	Exp_2	Combined	Exp_1	Exp_2	Combined	Exp_1	Exp_2	Combined
R2	0.9986	0.9964	0.9958	0.9989	0.9987	0.9987	0.9983	0.9982	0.9982
Number_points	86	171	257	75	142	217	34	61	95
MSEP	0.0734	0.1618		0.0673	0.1909		0.0048	0.0079	
ME	0.4179	0.1169		0.0072	0.0138		0.0561	0.0317	
SE	0.1490	0.0707		0.0136	0.0236		0.0317	0.0014	
NC	0.4388	0.8175		0.9826	0.9696		0.9408	0.9831	
RMSE			0.3651			0.3868			0.0834
F-test			1			1			1

DO validation

Scenario	Scen_AMO				
	Exp_1	Exp_2	Exp_3	Exp_4	Exp_5
R2	0.9981	0.9982	0.9947	0.9979	0.9964
Number_points	396	61	214	185	86
MSEP	0.2217	0.0078	0.6236	0.1697	0.0227
ME	0.1021	0.0274	0.2778	0.0425	0.1888
SE	0.2531	0.0014	0.2132	0.0236	0.4579
NC	0.6447	0.9874	0.5124	0.9391	0.3628
RMSE	0.4721	0.0897	0.7934	0.4142	0.1524
F-test	0	1	0	1	0

N_2O calibration

Scenario	Scen_An_HB			Scen_AMO				Scen_AMO, Scen_An_AOB			
	η_{HD}			ϵ_{AOB}				$\eta_{NOR}, K_{AOB, HNO_2}, K_{AOB, NH_2OH, ND}$			
Parameters Estimated	Exp_1	Exp_2	Combined	Exp_1	Exp_2	Exp_3	Combined	Exp_1	Exp_2	Exp_3	Combined
R2	0.9783	0.9869	0.9779	0.6503	0.6211	0.9255	0.9974	0.9892	0.9728	0.998	0.9979
Number_points	208	240	448	315	230	192	737	284	214	70	568
MSEP	0.0022	0.0003		0.0001	0.0001	0.0001		0.0001	0.0001	0.0001	
ME	0.0664	0.3456		0.1331	0.1515	0.6136		0.1461	0.0073	0.0300	
SE	0.0030	0.0767		0.0622	0.3636	0.0002		0.3661	0.7190	0.0266	
NC	0.9350	0.5805		0.8074	0.4886	0.3882		0.4909	0.2784	0.9574	
RMSE			0.0342				0.0007				0.0019
F-test			1				1				1

N_2O validation

Scenario	Scen_AMO, Scen_An_AOB		
	Exp_1	Exp_2	Exp_3
R2	0.9618	0.9692	0.9958
Number_points	396	261	60
MSEP	0.0001	0.1416	0.0001
ME	0.3234	0.4641	0.2421
SE	0.0526	0.0182	0.4015
NC	0.625	0.5198	0.3692
RMSE	0.0011	0.3777	0.0033
F-test	1	0	1

Section S6 – AOB-driven N₂O production from primary N-substrates

Biotically driven N₂O production associated to NH₄⁺ oxidation

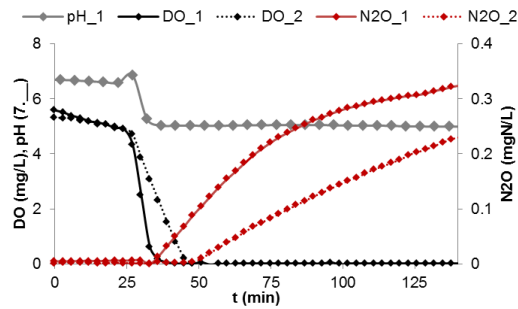


Figure S6-1 – Biotically-driven N₂O production from NH₄⁺ oxidation. VSS₁ = 0.3, VSS₂ = 0.13g/L yielded similar specific N₂O production rates: N₂O_{R1} = 0.21 and N₂O_{R2} = 0.24 mgN₂O-N/gVSS.min.

Role of NH₄⁺, NO₂⁻ and NH₂OH on anoxic N₂O production

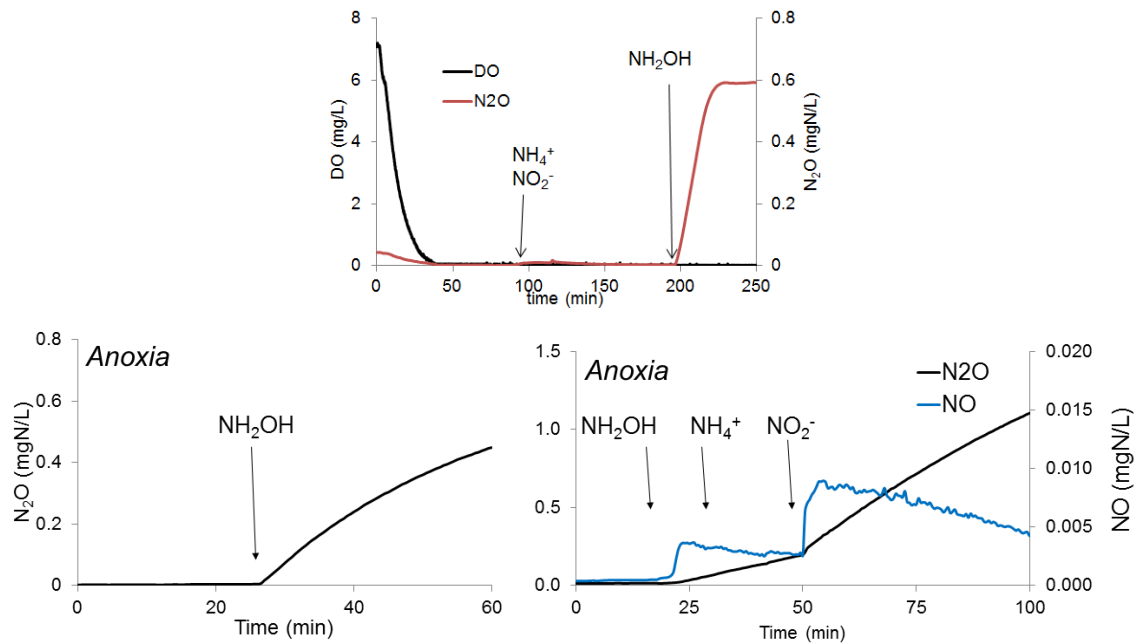


Figure S6-2 – (Top) Biotically-driven N₂O production from anoxic NH₂OH oxidation. (Bottom) N₂O and NO liquid concentrations from anoxic NH₂OH oxidation (left, NO₂⁻ < 0.05 mgN/L at the end of the experiment), and anoxic NH₂OH oxidation followed by NH₄⁺ and NO₂⁻ addition (right).

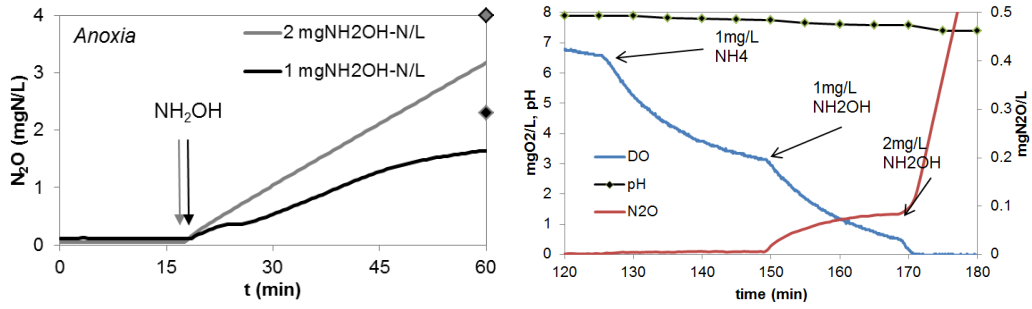


Figure S6-3 – (Left) N₂O concentration after anoxic NH₂OH spikes under excess NO₂⁻ (Markers, final N₂O concentrations). (Rigth) DO, pH and N₂O profiles after aerobic NH₄⁺ (1mgN/L), NH₂OH (1 and 2 mgN/L) spikes (Scen_HAO).

Under NO₂⁻ excess a NH₂OH spike yielded more N₂O than the corresponding NH₂OH added, indicating a combined NH₂OH and NO₂⁻ anoxic reaction (**Figure S6-4**).

Table S6-1 – N₂O production rates from two duplicate experiments of aerobic NH₄⁺ pulses, aerobic NH₂OH pulses, low DO NH₂OH pulses, anoxic NH₂OH pulses.

N2O_R (mgN2O-N/gVSS.min)		
Pulse	NG1	NG2
1 NH4	0.0008	0.0007
1 NH2OH	0.027	0.033
2 NH2OH @_limit_DO	0.023	0.033
< 2 NH2OH_anox	0.22	0.13

Abiotic N₂O production

To study the effect of HNO₂, NH₂OH and pH on abiotic N₂O production a factorial experimental design is constructed (Table S6-2). Results showed that in the absence of NO₂⁻, NH₂OH-driven abiotic N₂O production only occurs at very high pH (≥ 8.7) (Figure S6-4). Coupling HNO₂ and NH₂OH produced N₂O at: high pH (≥ 8) + high NH₂OH (≥ 0.5 mgN/L). Therefore high NO₂⁻ and NH₂OH concentrations are necessary, outside the range of typical wastewater systems (pH > 8.4, NO₂⁻ > 500 mgN/L, NH₂OH ≥ 0.5 mgN/L).

Table S6-2 - Factorial experimental design to study abiotic N₂O production.

HNO ₂ (µgN/L)	0	0.2	2	20	100
NH ₂ OH (mgN/L)	0	0.05	0.2	0.5	2
pH	6.5	7.25	8	8.7	9.4

Overall, the substrate concentrations necessary to produce N₂O abiotically are outside the range of the experiments design to calibrate the NDHA model: high pH, high NO₂⁻ and high NH₂OH.

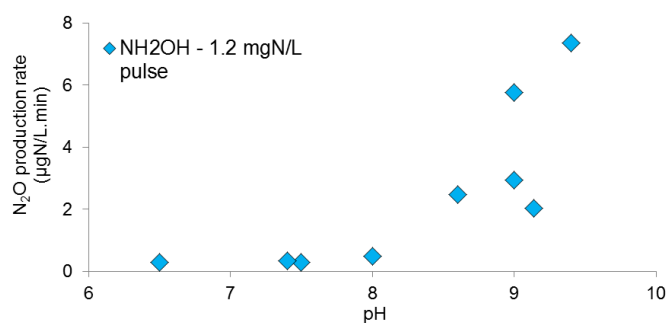


Figure S6-4 - Abiotic N₂O production rates for NH₂OH pulses (1.2 mgN/L) at varying pH.

Section S7 – Pathway contribution to total N₂O pool during model fitting

Based on the calibrated NDHA model the contribution of each pathway to the total N₂O production was analysed under various scenarios. During NH₄⁺ oxidation at high DO the NN pathway was responsible for all the N₂O produced as the ND and ND pathways are highly inhibited (Figure S7-1). The NN contribution is directly related to NH₂OH, thus when NH₄⁺ is depleted the NN contribution tapers off. As the DO level decreased the contribution of ND increased as both NH₂OH and FNA were present. All the NH₂OH left after reaching anoxia yielded N₂O from both the NN and ND pathways. Even under anoxia the NN pathway is still active but at a much lower rate than the ND pathway which clearly outcompeted the NH₂OH uptake in the presence of FNA, becoming the dominant N₂O producing pathway in the transition to anoxia. The HD pathway followed a similar trend to ND but at much lower rates as no external carbon was added.

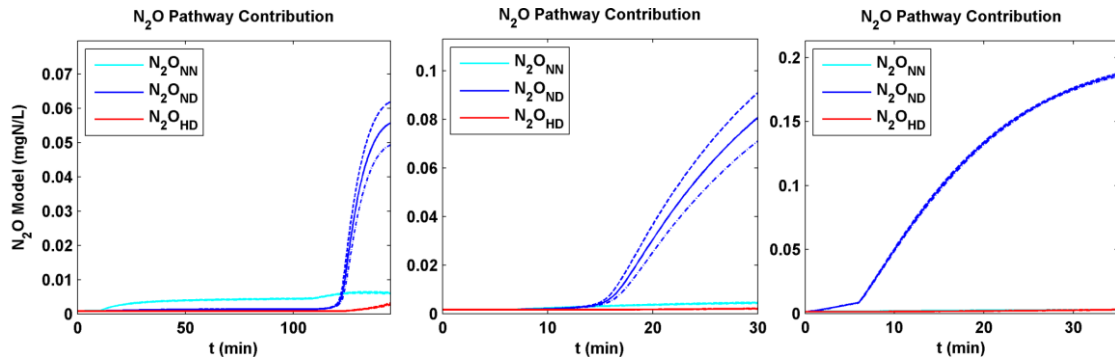


Figure S7-1 – Pathway contribution to the total N₂O pool and 95% CI from calibrated parameters for: (Left, Middle) Scen_AMO (NH₄⁺ pulses, Aerobic → anoxic), (Right) Scen_HAO (NH₂OH pulse, anoxic).

Section S8 – NDHA model evaluation

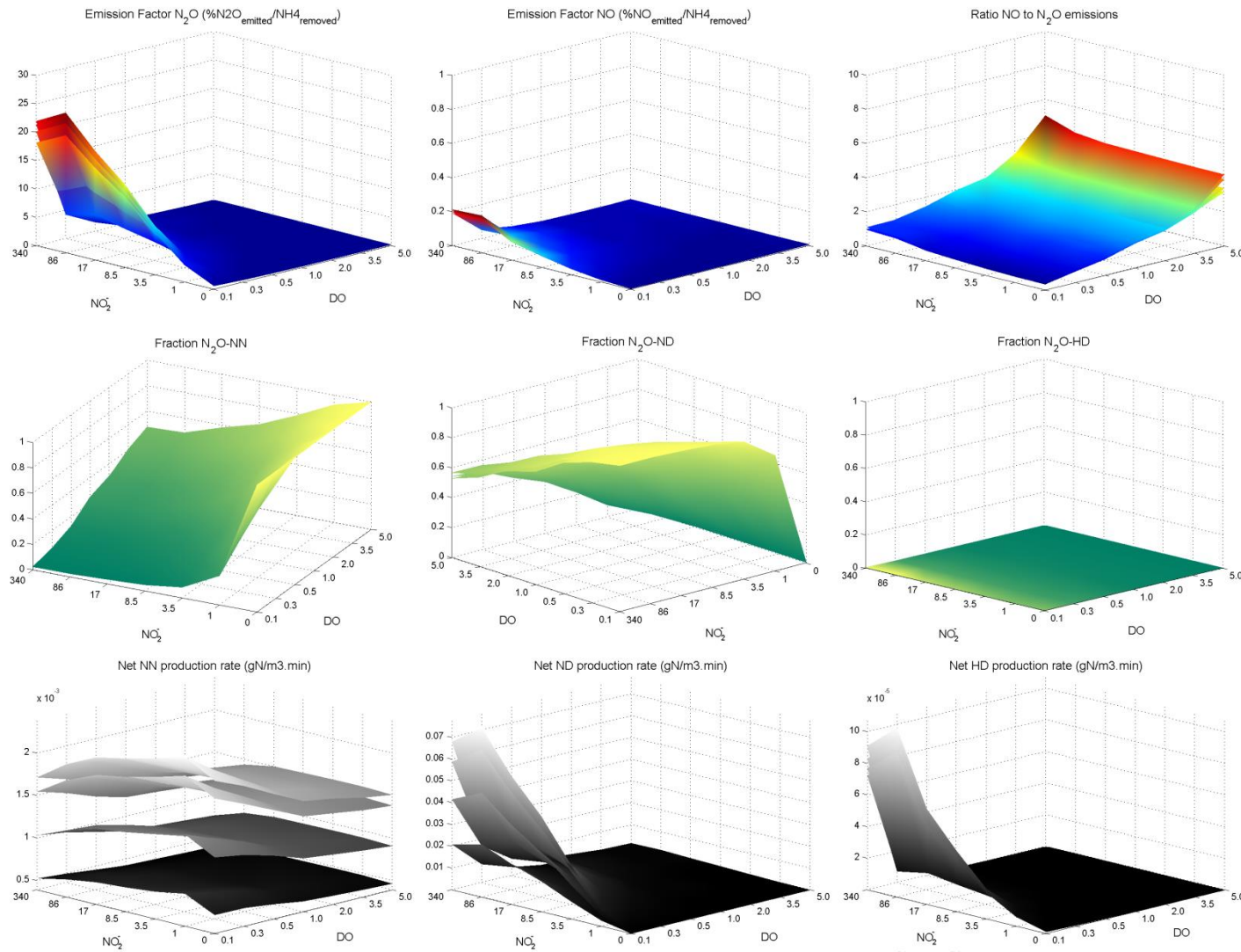


Figure S8-1 – Scenario analysis for model evaluation with best-fit parameters. Simulations were run under constant DO (0.1 - 0.3 - 0.5 - 1.0 - 2.0 - 3.5 - 5.0 mg/L), NO_2^- (0 - 1 - 3.5 - 8.5 - 17 - 86 - 340 mgN/L) and NH_4^+ (2.4 - 7.0 - 24 - 70 mgN/L). Top: (from left to right) N_2O , NO and NO/ N_2O emission factor (% $\text{N}_2\text{O}/\text{NH}_4^+$). Middle: NN, ND and HD Pathway contribution (-). Bottom: Net NN, ND and HD production rate ($\text{gN/m}^3\cdot\text{min}$).

Section S9 – Uncertainty propagation during NH_4^+ oxidation

The default uncertainty was propagated for all model parameters and compared to the uncertainty of only the calibrated parameters (μ_{NOB} , k_{H} , $\mu_{\text{AOB.AMO}}$, $K_{\text{AOB.NH}_3}$ and $K_{\text{AOB.O}_2.\text{AMO}}$). A similar width of the 95% CI indicate that the model outputs were very sensitive to the parameter subset calibrated. After calibration the uncertainty obtained for those five parameters was also propagated highlighting a significant decrease of the prediction uncertainty, not only for the main N-species but also for N_2O . A precise calibration of NH_4^+ removal will help reduce the uncertainty associated to N_2O production, which will benefit the experimental designs focused on N_2O calibrations.

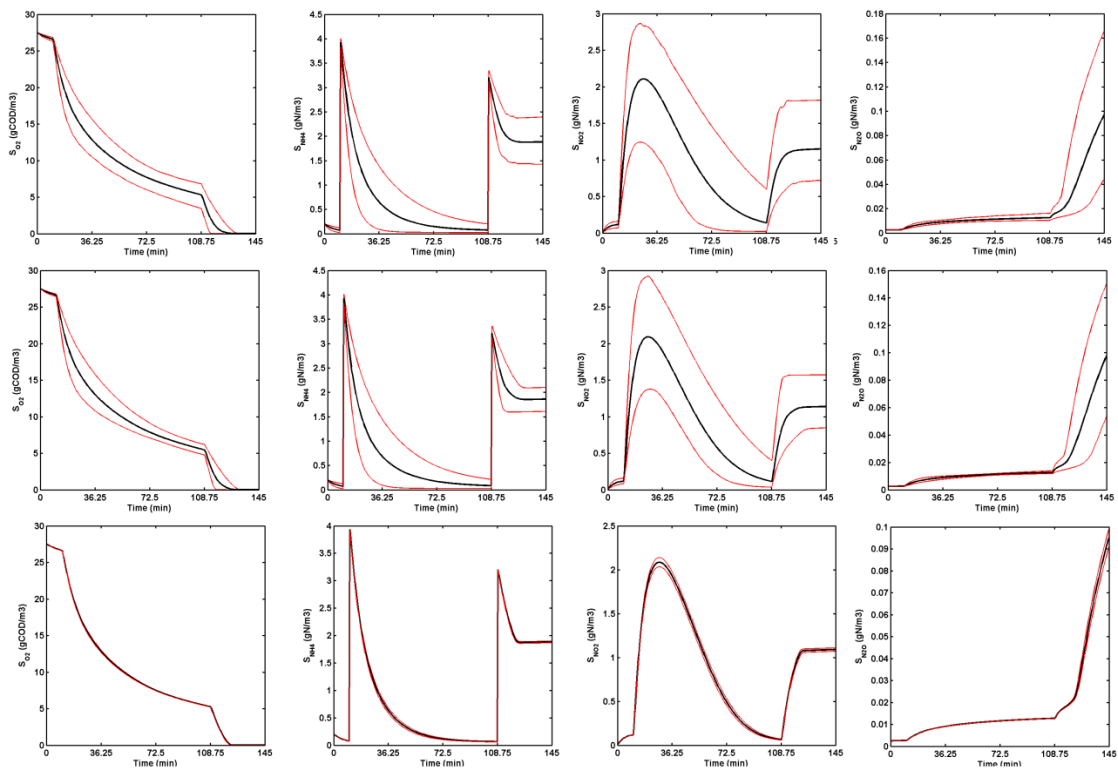


Figure S9-1 – Uncertainty propagation for an experiment of Scen_AMO (x2 NH_4^+ pulses) Top panels: Default uncertainty for all model parameters. Middle: Default uncertainty only for parameters estimated with the DO dataset (μ_{NOB} , k_{H} , $\mu_{\text{AOB.AMO}}$, $K_{\text{AOB.NH}_3}$ and $K_{\text{AOB.O}_2.\text{AMO}}$). Bottom: Uncertainty from DO calibration only for parameters estimated with the DO dataset (Table 2).

Section S10 – NDHA model

Component (i) ▶ Process (j) ▼	1 S _S	2 S _{O2}	3 S _{NH3}	4 S _{NH2OH}	5 S _{HNO2}	6 S _{NO3}	7 S _{NO}	8 S _{N2O}	9 S _{N2}	10 S _{IC}	11 X _{B,AOB}	12 X _{B,NOB}	13 X _{B,H}	14 X _S	15 X _I
AOB growth															
Aerobic_AMO 1		-1.14	-1	1						-1/14					
Aerobic_HAO* 2			-i _{NXB}	-1/Y _{AOB}			1/Y _{AOB}			-1/14(i _{NXB})	1				
Aerobic_HAO 3		-((2.29-Y _{AOB})/Y _{AOB})	-i _{NXB}	-1/Y _{AOB}	1/Y _{AOB}					-1/14(i _{NXB} -1/Y _{AOB})	1				
Anox_A_NIR 4				-1	-3		4			3/14					
Anox_A_NOR 5				-1			-2	3		-1/14					
NOB growth															
Aer_NOB_growth 6		-((1.14-Y _{NOB})/Y _{NOB})	-i _{NXB}		-1/Y _{NOB}	1/Y _{NOB}				-i _{NXB} /14		1			
HB growth															
Aerobic_H_growth 7	-1/Y _{HB}	-((1-Y _{HB})/Y _{HB})	-i _{NXB}							-i _{NXB} /14			1		
Anox_H_NAR 8	-1/Y _{HB}		-i _{NXB}		((1-Y _{HB})/(1.14·Y _{HB}))	-((1-Y _{HB})/(1.14·Y _{HB}))				-i _{NXB} /14			1		
Anox_H_NIR 9	-1/Y _{HB}		-i _{NXB}		-((1-Y _{HB})/(0.57·Y _{HB}))		((1-Y _{HB})/(0.57·Y _{HB}))			-1/14(i _{NXB} ·(1-γ _{HB})/(0.57·γ _{HB}))			1		
Anox_H_NOR 10	-1/Y _{HB}		-i _{NXB}				-((1-Y _{HB})/(0.57·Y _{HB}))	((1-Y _{HB})/(0.57·Y _{HB}))		-i _{NXB} /14			1		
Anox_H_NOS 11	-1/Y _{HB}		-i _{NXB}				-((1-Y _{HB})/(0.57·Y _{HB}))	((1-Y _{HB})/(0.57·Y _{HB}))		-i _{NXB} /14			1		
Lysis															
AOB 12			i _{NXB} ·f _i ·i _{NXI} ·(1-f _i)·i _{NXS}							(i _{NXB} ·f _i ·i _{NXI} ·(1-f _i)·i _{NXS})/14	-1			1-f _{xi}	f _{xi}
NOB 13			i _{NXB} ·f _i ·i _{NXI} ·(1-f _i)·i _{NXS}							(i _{NXB} ·f _i ·i _{NXI} ·(1-f _i)·i _{NXS})/14		-1		1-f _{xi}	f _{xi}
HB 14			i _{NXB} ·f _i ·i _{NXI} ·(1-f _i)·i _{NXS}							(i _{NXB} ·f _i ·i _{NXI} ·(1-f _i)·i _{NXS})/14			-1	1-f _{xi}	f _{xi}
Hydrolysis															
Aerobic 15	1		i _{NXS}							i _{NXS} /14				-1	
Anoxic 16	1		i _{NXS}							i _{NXS} /14				-1	
Anaerobic 17	1		i _{NXS}							i _{NXS} /14				-1	
Aeration 18		1													
Stripping_N2O 19								-1							
Stripping_NO 20							-1								

Component (i) ▶		Process Rate (g·m ⁻³ ·s ⁻¹)
	Process (j) ▼	
AOB growth		
Aerobic_AMO	1	$\mu_{AMO}^{AOB} \cdot \frac{S_{O_2}}{S_{O_2} + K_{O_2,AMO}^{AOB}} \cdot \frac{S_{NH_3}}{S_{NH_3} + K_{NH_3}^{AOB} + S_{NH_3}^2 / K_{1,NH_3}^{AOB}} \cdot \frac{K_{1,HNO_2}^{AOB}}{S_{HNO_2} + K_{1,HNO_2}^{AOB}} \cdot X_{AOB}$
Aerobic_HAO*	2	$\mu_{HAO}^{AOB} \cdot \varepsilon_{AOB} \cdot \frac{S_{NH_2OH}}{S_{NH_2OH} + K_{NH_2OH}^{AOB}} \cdot X_{AOB}$
Aerobic_HAO	3	$\mu_{HAO}^{AOB} \cdot (1 - \varepsilon_{AOB}) \cdot \frac{S_{O_2}}{S_{O_2} + K_{O_2,HAO}^{AOB}} \cdot \frac{S_{NH_2OH}}{S_{NH_2OH} + K_{NH_2OH}^{AOB}} \cdot X_{AOB}$
Anox_A_NIR	4	$\mu_{HAO}^{AOB} \cdot \eta_{NIR} \cdot \frac{K_{1,O_2}^{AOB}}{S_{O_2} + K_{1,O_2}^{AOB}} \cdot \frac{S_{NH_2OH}}{S_{NH_2OH} + K_{NH_2OH,ND}^{AOB}} \cdot \frac{S_{HNO_2}}{S_{HNO_2} + K_{HNO_2}^{AOB}} \cdot X_{AOB}$
Anox_A_NOR	5	$\mu_{HAO}^{AOB} \cdot \eta_{NOR} \cdot \frac{S_{NH_2OH}}{S_{NH_2OH} + K_{NH_2OH,ND}^{AOB}} \cdot \frac{S_{NO}}{S_{NO} + K_{NO}^{AOB}} \cdot X_{AOB}$
NOB growth		
Aer_NOB_growth	6	$\mu_{NOB}^{NOB} \cdot \frac{S_{O_2}}{S_{O_2} + K_{O_2}^{NOB}} \cdot \frac{S_{HNO_2}}{S_{HNO_2} + K_{HNO_2}^{NOB} + S_{HNO_2}^2 / K_{1,HNO_2}^{NOB}} \cdot \frac{K_{1,NH_3}^{NOB}}{S_{NH_3} + K_{1,NH_3}^{NOB}} \cdot X_{NOB}$
HB growth		
Aerobic_H_growth	7	$\mu_{HB}^{HB} \cdot \frac{S_{O_2}}{S_{O_2} + K_{O_2}^{HB}} \cdot \frac{S_{NH_4}}{S_{NH_4} + K_{NH_4}^{HB}} \cdot \frac{S_S}{S_S + K_S^{HB}} \cdot X_{HB}$
Anox_H_NAR	8	$\mu_{NAR}^{HB} \cdot \frac{K_{1,O_2,NAR}^{HB}}{S_{O_2} + K_{1,O_2,NAR}^{HB}} \cdot \frac{S_S}{S_S + K_{S,NAR}^{HB}} \cdot \frac{S_{NH_4}}{S_{NH_4} + K_{NH_4}^{HB}} \cdot \frac{S_{NO_3}}{S_{NO_3} + K_{NO_3}^{HB}} \cdot X_{HB}$
Anox_H_NIR	9	$\mu_{NIR}^{HB} \cdot \frac{K_{1,O_2,NIR}^{HB}}{S_{O_2} + K_{1,O_2,NIR}^{HB}} \cdot \frac{K_{1,NO,NIR}^{HB}}{S_{NO} + K_{1,NO,NIR}^{HB}} \cdot \frac{S_S}{S_S + K_{S,NIR}^{HB}} \cdot \frac{S_{NH_4}}{S_{NH_4} + K_{NH_4}^{HB}} \cdot \frac{S_{NO_2}}{S_{NO_2} + K_{NO_2}^{HB}} \cdot X_{HB}$
Anox_H_NOR	10	$\mu_{NOR}^{HB} \cdot \frac{K_{1,O_2,NOR}^{HB}}{S_{O_2} + K_{1,O_2,NOR}^{HB}} \cdot \frac{S_S}{S_S + K_{S,NOR}^{HB}} \cdot \frac{S_{NH_4}}{S_{NH_4} + K_{NH_4}^{HB}} \cdot \frac{S_{NO}}{S_{NO} + K_{NO}^{HB} + S_{NO}^2 / K_{1,NO,NOR}^{HB}} \cdot X_{HB}$
Anox_H_NOS	11	$\mu_{NOS}^{HB} \cdot \frac{K_{1,O_2,NOS}^{HB}}{S_{O_2} + K_{1,O_2,NOS}^{HB}} \cdot \frac{K_{1,NO,NOS}^{HB}}{S_{NO} + K_{1,NO,NOS}^{HB}} \cdot \frac{S_S}{S_S + K_{S,NOS}^{HB}} \cdot \frac{S_{NH_4}}{S_{NH_4} + K_{NH_4}^{HB}} \cdot \frac{S_{N_2O}}{S_{N_2O} + K_{N_2O}^{HB}} \cdot X_{HB}$
Lysis		
AOB	12	$b_{AOB} \cdot \left(\frac{S_{O_2}}{S_{O_2} + K_{O_2,b}} + \eta_b \cdot \frac{K_{O_2,b}}{K_{O_2,b} + S_{O_2}} \cdot \frac{S_{NOx}}{K_{NOx} + S_{NOx}} \right) \cdot X_{AOB}$
NOB	13	$b_{NOB} \cdot \left(\frac{S_{O_2}}{S_{O_2} + K_{O_2,b}} + \eta_b \cdot \frac{K_{O_2,b}}{K_{O_2,b} + S_{O_2}} \cdot \frac{S_{NOx}}{K_{NOx} + S_{NOx}} \right) \cdot X_{NOB}$
HB	14	$b_{HB} \cdot \left(\frac{S_{O_2}}{S_{O_2} + K_{O_2,b}} + \eta_b \cdot \frac{K_{O_2,b}}{K_{O_2,b} + S_{O_2}} \cdot \frac{S_{NOx}}{K_{NOx} + S_{NOx}} \right) \cdot X_{HB}$
Hydrolysis		
Aerobic	15	$k_H \cdot \frac{X_S / X_{BH}}{K_X + X_S / X_{BH}} \cdot \frac{S_{O_2}}{K_{O_2}^{HB} + S_{O_2}} \cdot X_{HB}$
Anoxic	16	$k_H \cdot \eta_{ANOX} \cdot \frac{X_S / X_{BH}}{K_X + X_S / X_{BH}} \cdot \frac{K_{O_2}^{HB}}{K_{O_2}^{HB} + S_{O_2}} \cdot \frac{S_{NO_3}}{K_{NO_3}^{HB} + S_{NO_3}} \cdot X_{HB}$
Anaerobic	17	$k_H \cdot \eta_{AN} \cdot \frac{X_S / X_{BH}}{K_X + X_S / X_{BH}} \cdot \frac{K_{O_2}^{HB}}{K_{O_2}^{HB} + S_{O_2}} \cdot \frac{K_{NO_3}^{HB}}{K_{NO_3}^{HB} + S_{NO_3}} \cdot X_{HB}$
Aeration	18	$K_{la,O_2} \cdot (S_{O_2}^* - S_{O_2})$
Stripping_N ₂ O	19	$K_{la,N_2O} \cdot (S_{N_2O} - S_{N_2O}^*)$
Stripping_NO	20	$K_{la,NO} \cdot (S_{NO} - S_{NO}^*)$

Parameter	Definition	Value	Estimated	CV (%)	Units	Ref.
AOB						
$K_{AOB.NH_2OH}$	S_{NH_2OH} affinity for AOB	0.3			mgN/L	(1)
$K_{AOB.NH_2OH.ND}$	S_{NH_2OH} affinity for AOB during NO reduction	0.3	0.25	1.8	mgN/L	(1)
$K_{AOB.NH_3}$	S_{NH_3} affinity for AOB	0.0075	0.1216	3.9	mgN/L	
$K_{AOB.NO.ND}$	S_{NO} affinity for AOB	0.004			mgN/L	(3)
$K_{AOB.HNO_2}$	S_{HNO_2} affinity for AOB	0.0001	0.000672	4.4	mgN/L	(4)
$K_{AOB.O_2.AMO}$	S_{O_2} AMO-mediated affinity constant	0.4	0.225	7	mgO ₂ /L	(5)
$K_{AOB.O_2.HAO}$	S_{O_2} HAO-mediated affinity constant	0.4			mgO ₂ /L	(5)
$K_{AOB.O_2.i}$	S_{O_2} inhibition constant for AOB	0.1			mgO ₂ /L	(7)
$K_{AOB.i.NH_3}$	S_{NH_3} inhibition constant for AOB	10			mgN/L	(6)
$K_{AOB.i.HNO_2}$	S_{HNO_2} inhibition constant for AOB	0.75			mgN/L	(6)
ϵ_{AOB}	Reduction factor for HAO-mediated maximum reaction rate	0.001	0.000483	1.1	(-)	New
η_{NIR}	Anoxic reduction factor for NO ₂ reduction	0.15			(-)	(7)
η_{NOR}	Reduction factor for NO reduction	0.15	0.157	3.2	(-)	(7)
$\mu_{AOB.AMO}$	Maximum AMO-mediated reaction rate	0.78	0.49	2	1/d	(2)
$\mu_{AOB.HAO}$	Maximum HAO-mediated reaction rate	0.78			1/d	(2)
b_{AOB}	Endogenous decay rate for AOB	0.096			1/d	(2)
Y_{AOB}	Yield coefficient for AOB	0.18			mgCOD/mgN	(2)
NOB						
$K_{NOB.HNO_2}$	S_{HNO_2} affinity for NOB	0.0001			mgN/L	(2)
$K_{NOB.O_2}$	S_{O_2} affinity constant for NOB	1.2			mgO ₂ /L	(2)
$K_{NOB.i.NH_3}$	S_{NH_3} inhibition constant for NOB	0.5			mgN/L	(6)
$K_{NOB.i.HNO_2}$	S_{HNO_2} inhibition constant for NOB	0.1			mgN/L	(6)
μ_{NOB}	Maximum NOB growth	0.78	0.66	1	1/d	(2)
b_{NOB}	Endogenous decay rate for NOB	0.096			1/d	(2)
Y_{NOB}	Yield coefficient for NOB	0.06			mgCOD/mgN	(2)
Others						
f_{XI}	Fraction of inerts in biomass	0.08			(-)	(2)
i_{NXB}	Nitrogen content of biomass	0.086			mgN/mgCOD	(2)
i_{NXI}	Nitrogen content of inerts	0.02			mgN/mgCOD	(2)
i_{NXS}	Nitrogen content of particulate	0.06			mgN/mgCOD	(2)
η_b	Anoxic reduction factor of endogenous decay	0.33			(-)	(5)
$K_{O_2.b}$	S_{O_2} affinity constant of endogenous decay	0.2			mgO ₂ /L	(5)
K_{NOx}	$S_{NO_2}+S_{NO_3}$ affinity constant of endogenous decay	0.2			mgN/L	(5)
k_H	Hydrolysis rate	2.21	2.01	0.9	1/d	(2)
K_X	Affinity constant for hydrolysis	0.15			mgCOD/mgC	(2)
η_{anox}	Anoxic hydrolysis factor	0.4			(-)	(5)
η_{anaer}	Anaerobic hydrolysis factor	0.4			(-)	(5)

Parameter	Definition	Value	Estimated	CV (%Units)	Ref.
HB					
$K_{HB.NH4}$	S_NH4 affinity constant for HB	0.01		mgN/L	(2)
$K_{HB.NO3}$	S_NO3 affinity constant for HB	0.2		mgN/L	(2)
$K_{HB.NO2}$	S_NO2 affinity constant for HB	0.2		mgN/L	(2)
$K_{HB.NO}$	S_NO affinity constant for HB	0.05		mgN/L	(2)
$K_{HB.N2O}$	S_N2O affinity constant for HB	0.05		mgN/L	(2)
$K_{HB.S}$	S_S affinity constant for HB	20		mgCOD/L	(2)
$K_{HB.S.NAR}$	S_S affinity constant for S_NO3 reduction	20		mgCOD/L	(2)
$K_{HB.S.NIR}$	S_S affinity constant for S_NO2 reduction	20		mgCOD/L	(2)
$K_{HB.S.NOR}$	S_S affinity constant for S_NO reduction	20		mgCOD/L	(2)
$K_{HB.S.NOS}$	S_S affinity constant for S_N2O reduction	40		mgCOD/L	(2)
$K_{HB.O2}$	S_O2 affinity constant for HB	0.1		mgO2/L	(2)
$K_{HB.O2.i.NAR}$	S_O2 inhibition constant for S_NO3 reduction	0.1		mgO2/L	(2)
$K_{HB.O2.i.NIR}$	S_O2 inhibition constant for S_NO2 reduction	0.1		mgO2/L	(2)
$K_{HB.O2.i.NOR}$	S_O2 inhibition constant for S_NO reduction	0.1		mgO2/L	(2)
$K_{HB.O2.i.NOS}$	S_O2 inhibition constant for S_N2O reduction	0.1		mgO2/L	(2)
$K_{HB.NO.i.NIR}$	S_NO inhibition constant for S_NO2 reduction	0.5		mgN/L	(2)
$K_{HB.NO.i.NOR}$	S_NO inhibition constant for S_NO reduction	0.3		mgN/L	(2)
$K_{HB.NO.i.NOS}$	S_NO inhibition constant for S_N2O reduction	0.075		mgN/L	(2)
μ_{HB}	Maximum HB growth rate	6.24		1/d	(2)
$\mu_{HB.NAR}$	Maximum NO3-reduction reaction rate	1.754		1/d	(2)
$\mu_{HB.NIR}$	Maximum NO2-reduction reaction rate	1		1/d	(2)
$\mu_{HB.NOR}$	Maximum NO-reduction reaction rate	2.18		1/d	(2)
$\mu_{HB.NOS}$	Maximum N2O-reduction reaction rate	2.18		1/d	(2)
η_{HD}	Reduction factor for HB denitrification	0.2	0.05	(-)	(-)
b_{HB}	Endogenous decay rate for HB	0.41		1/d	(2)
Y_{HB}	Yield coefficient for HB	0.6		mgCOD/mgCOD	(2)

(1) Assumed, (2) Hiatt-Grady 2008, (3) Spérandio 2016, (4) Domingo-Felez 2017, (5) Lisha Guo 2014, (6) Park 2010, (7) Ni 2011,

References

- Akaike H. 1974. A new look at the statistical model identification. *IEEE Trans. Automat. Contr.* **19**:716–723.
- Böttcher B, Koops HP. 1994. Growth of lithotrophic ammonia-oxidizing bacteria on hydroxylamine. *FEMS Microbiol. Lett.* **122**:263–266.
- Brouwer H, Klapwijk A, Keesman KJ. 1998. Identification of activated sludge and wastewater characteristics using respirometric batch-experiments. *Water Res.* **32**:1240–1254.
- de Bruijn P, van de Graaf AA, Jetten MSM, Robertson LA, Kuenen JG. 1995. Growth of *Nitrosomonas europaea* on hydroxylamine. *FEMS Microbiol. Lett.* **125**:179–184.
- Cantera JLL, Stein LY. 2007. Role of nitrite reductase in the ammonia-oxidizing pathway of *Nitrosomonas europaea*. *Arch. Microbiol.* **188**:349–54.
- Chandran K, Smets BF. 2008. Biokinetic Characterization of the Acceleration Phase in Autotrophic Ammonia Oxidation. *Water Environ. Res.* **80**:732–739.
- Ding X, Zhao J, Hu B, Chen Y, Ge G, Li X, Wang S, Gao K, Tian X. 2016. Mathematical modeling of nitrous oxide production in an anaerobic/oxic/anoxic process. *Bioresour. Technol.* **222**:39–48.
- Dochain D, Vanrolleghem PA. 2001. Dynamic Modelling and Estimation in Wastewater Treatment Processes. London, UK: IWA Publishing.
- Domingo-Félez C, Smets BF. 2016. A consilience model to describe N₂O production during biological N removal. *Environ. Sci. Water Res. Technol.* **2**:923–930.
- Frear DS, Burrell RC. 1955. Spectrophotometric Method for Determining Hydroxylamine Reductase Activity in Higher Plants. *Anal. Chem.* **27**:1664–1665.
- Guisasola A, Chandran K, Smets BF, Baeza JA, Carrera J, Lafuente J. 2006. Observation and mathematical description of the acceleration phenomenon in batch respirograms associated with ammonium oxidation. *Water Sci. Technol.* **54**:181–188.
- Holmberg A. 1982. On the practical identifiability of microbial growth models incorporating Michaelis-Menten type nonlinearities. *Math. Biosci.* **62**:23–43.
- Hooper AB, Terry KR. 1979. Hydroxylamine oxidoreductase of *Nitrosomonas*. Production of nitric oxide from hydroxylamine. *BBA - Enzymol.* **571**:12–20.
- Law Y, Lant P, Yuan Z. 2011. The effect of pH on N₂O production under aerobic conditions in a partial nitrification system. *Water Res.* **45**:5934–44.
- Machado VC, Tapia G, Gabriel D, Lafuente J, Baeza JA. 2009. Systematic identifiability study based on the Fisher Information Matrix for reducing the number of parameters calibration of an activated sludge model. *Environ. Model. Softw.* **24**:1274–1284.
- Ni B-J, Peng L, Law Y, Guo J, Yuan Z. 2014. Modeling of Nitrous Oxide Production by Autotrophic Ammonia-Oxidizing Bacteria with Multiple Production Pathways. *Environ. Sci. Technol.* **48**:3916–24.
- Ni B-J, Rusalleda M, Pellicer-Nàcher C, Smets BF. 2011. Modeling nitrous oxide production during biological nitrogen removal via nitrification and denitrification: extensions to the general ASM models. *Environ. Sci. Technol.* **45**:7768–76.
- Ni B-J, Ye L, Law Y, Byers C, Yuan Z. 2013a. Mathematical Modeling of Nitrous Oxide (N₂O) Emissions from Full-Scale Wastewater Treatment Plants. *Environ. Sci. Technol.* **47**:7795–7803.
- Ni B-J, Yuan Z, Chandran K, Vanrolleghem PA, Murthy S. 2013b. Evaluating four mathematical models for nitrous oxide production by autotrophic ammonia-oxidizing bacteria. *Biotechnol. Bioeng.* **110**:153–63.

- Pocquet M, Wu Z, Queinnec I, Spérandio M. 2016. A two pathway model for N₂O emissions by ammonium oxidizing bacteria supported by the NO/N₂O variation. *Water Res.* **88**:948–959.
- Sayavedra-Soto LA, Hommes NG, Russell SA, Arp DJ. 1996. Induction of ammonia monooxygenase and hydroxylamine oxidoreductase mRNAs by ammonium in *Nitrosomonas europaea*. *Mol. Microbiol.* **20**:541–548.
- Sin G, Gernaey K V, Neumann MB, van Loosdrecht MCM, Gujer W. 2009. Uncertainty analysis in WWTP model applications: a critical discussion using an example from design. *Water Res.* **43**:2894–906.
- Upadhyay AK, Hooper AB, Hendrich MP. 2006. NO reductase activity of the tetraheme cytochrome C554 of *Nitrosomonas europaea*. *J. Am. Chem. Soc.* **128**:4330–7.